Carbohydrate Polymers 214 (2019) 234–249

Contents lists available at ScienceDirect

Carbohydrate Polymers

journal homepage: www.elsevier.com/locate/carbpol

An injectable mechanically robust hydrogel of Kappa-carrageenan-dopamine functionalized graphene oxide for promoting cell growth

Hamidreza Mokhtari, Mahshid Kharaziha*, Fathallah Karimzadeh, Shima Tavakoli

Department of Materials Engineering, Isfahan University of Technology, Isfahan 84156-83111, Iran

ARTICLE INFO

Keywords:
Shear thinning
Self-healing
Nanohybrid hydrogels
Kappa-carrageenan
Graphene oxide
Dopamine

ABSTRACT

An injectable nanohybrid hydrogel with robust mechanical properties was developed based on Methacrylate-Kappa-carrageenan (KaMA)-dopamine functionalized graphene oxide (GOPD) for soft tissue engineering. KaMA-GOPD hydrogels revealed shear-thinning behavior and injectability through interaction of active catechol groups of dopamine with other moieties in the structure of hydrogels. In addition, these interactions promoted mechanical properties of hydrogels, depending on the GOPD content. Noticeably, encapsulation of 20 wt.% GOPD significantly enhanced compressive strength (8-folds) and toughness (6-folds) of KaMA. Furthermore, the hybrid hydrogel consisting of 20 wt.% GOPD significantly reduced energy loss from 70% (at KaMA) to about 61%, after a two-cycle compression test, while significantly enhanced recovery of the KaMA structure. Reinforcing the KaMA with 20 wt.% GOPD resulted in enhanced fibroblast proliferation (2.5-times) and spreading (5.7 times) after 5 days of culture. Based on these findings, KaMA-GOPD hydrogel could be used for cell delivery through the injection process and applied as a suitable bio-ink for 3D-bioproiting process.

1. Introduction

Recently, soft tissue engineering has been recognized as an intersection point among engineering, medicine, and biology to repair damages of soft tissue (Stratton et al., 2018). Current medical therapy is usually invasive surgery such as tumor resection and large traumatic injuries (Rnjak-Kovacina et al., 2015). To overcome the limitations of the current therapies, soft tissue engineering has been developed as a new strategy for restoring diseased soft tissues and organs, pointing repair of volume loss (Rnjak-Kovacina et al., 2015; Yuksel, Choo, Wettergreen, & Liebschner, 2005). In this field, various types of biomaterials with appropriate properties have been utilized in order to heal and regenerate the damaged tissue. However, this approach is usually accompanied with invasive surgery for pasting biomaterials-based constructs, facing with side-effects such as post-operative bleeding, infection and damage to other nearby organs (Keller, Tahilramani, Flores-Gonzalez, Mahmood, & Haas, 2016; Pittet, Montandon, & Pittet, 2005). In this respect, injectable biomaterials are popular platforms to precisely fill the damaged area and facilitate tissue regeneration. Between them, thanks to unique properties of injectable hydrogels, consisting of high-water content, permeability to soluble factors such as oxygen, good biocompatibility, tunable biodegradability and ability to encapsulate cell and bio-macromolecules, they are extensively applied for soft tissue regeneration (Vunjak-Novakovic et al., 2010; Yu & Ding, 2008). Moreover, injectable hydrogels reveal excellent features that give them ability to closely mimic the natural living tissues and turned the hydrogels to unique scaffolds with a minimally invasive injection method (Kretlow, Klouda, & Mikos, 2007; Loebel, Rodell, Chen, & Burdick, 2017). Between various types of injectable hydrogels, shear-thinning injectable ones are capable of shielding encapsulated cells from high shear forces (Guvendiren, Lu, & Burdick, 2012). Shear-thinning hydrogels exhibit viscous flow under shear stress. When the stress is released, they recover depending on the time during relaxation (Guvendiren et al., 2012). This strange response attracts researcher to provide an alternative strategy for injectable hydrogel application and thereby improving outcome of cell-based therapeutics (Yang et al., 2012; Yang, Zhang, Yue, & Khademhosseini, 2017). Researchers have utilized different polymers for making injectable hydrogels that can be extruded and molded to the desired shapes (Diba, Pape et al., 2017; Diba, Wang, Kodger, Parsa, & Leeuwenburgh, 2017; Wang, Wang, Lu, Detamore, & Berkland, 2010). Kappa-carrageenan (κ-CA) is one of the biopolymers with great properties making it a suitable candidate for tissue engineering applications (Mihaila et al., 2013).

Kappa-carrageenan (κ-CA) extracted from red seaweeds possesses ester sulfate content of about 25–30% (Jiao, Yu, Zhang, & Ewart, 2011;

* Corresponding author.
E-mail address: kharaziha@cc.iut.ac.ir (M. Kharaziha).

https://doi.org/10.1016/j.carbpol.2019.03.030
Received 5 February 2019; Received in revised form 10 March 2019; Accepted 10 March 2019
Available online 12 March 2019
0144-8617/

Necas & Bartosikova, 2013). κ-CA has been proposed as a potential candidate for tissue engineering applications, owing to its gelation properties, mechanical strength and resembling chondroitin-4-sulphate and dermatan sulphate, which are major components of native extracellular matrices called glycosaminoglycan (GAGs) (Campo, Kawano, Silva, & Carvalho, 2009; Popa, Caridade, Mano, Reis, & Gomes, 2015). Moreover, the ionic crosslinking process of κ-CA using KCl could provide hydrogels with strong ionic interactions between sulfate groups and ions. Although ionic crosslinking process promoted mechanical strength and stiffness, it changes κ-CA to a brittle hydrogel (Thakur et al., 2016). Recently, Mihaila et al. (Mihaila et al., 2013) developed photo-crosslinkable κ-CA via methacrylate κ-CA (KaMA) and found that, the mixture of physical and chemical crosslinking procedure improved mechanical properties and promoting integrity of KaMA, while permitting maintenance of viable encapsulated cells. Recently, various researches have shown the successful generation of nanocomposite hydrogels based on κ-CA hydrogels consisting of silicate (Cross, Shah, Palani, Peak, & Gaharwar, 2018; Lokhande et al., 2018; Thakur et al., 2016), whitlockite (Yegappan et al., 2019) and metal oxide (Daniel-da-Silva et al., 2012; Thanusha et al., 2018). These nanocomposite hydrogels could improve mechanical properties of κ-CA and enhance the physiological stability. However, according to our knowledge, shear-thinning behavior of κ-CA- graphene oxide hydrogels have never been investigated.

Lately, graphene based materials have revealed great potentials for biomedical applications, due to their biocompatibility and unique electrical, mechanical and thermal properties (Chung et al., 2013; Paul et al., 2014; Shin et al., 2014). Graphene is a two-dimensional (2D) material composed of sp^2 hybridized carbon atoms with a single atom layer. The specific structure of graphene with high specific area and interaction between graphene as a reinforcement and polymer's chains makes it appropriate for development of nanocomposites (Chung et al., 2013). Between various derivations of graphene, graphene oxide (GO) consists of various functional groups such as hydroxyl, carboxyl and epoxy which make it a good reinforcing additive for various polymers and hydrogels applied for tissue engineering (Liao, Qu, Chu, Zhang, & Qian, 2015; Paul et al., 2014; Zhang et al., 2011). Del Giudice and Shen (2017) found that incorporation of special amounts of GO to water created shear-thinning behavior for Newtonian fluid like water, owing to the functional groups on GO surface. Recently, GO was also applied as an reinforcing agent for hydrogels to improve mechanical properties (Das et al., 2013; Paul et al., 2014) and develop Newtonian solution by interaction of sacrificing electrostatic band between GO and polymeric structure (Kim & Lee, 2014). However, results showed that the interaction between GO nanosheets and hydrogel matrix was slightly weak (Kim & Lee, 2014; Paul et al., 2014). In this regard, polydopamine (PD) has been introduced as a mussel-inspired adhesive material which has been widely applied to develop robust and significant hydrogels (Han et al., 2017; Lee, Dellatore, Miller, & Messersmith, 2007).

PD is usually prepared via the oxidation of the catechol groups of dopamine (DA) by oxygen or oxidant reagents such as $FeCl_3$ and $NaOI_4$. Moreover, the thickness of PD can be adjusted by changing the time of cross-linking or oxidizing of the catechol groups. It could provide an advantage to obtain ultrathin PD film on the surface of nanomaterials to achieve excellent binding kinetics (Luo, Jiang, & Liu, 2013). PD has recently been applied as a thin layer on the surface of GO nanosheets in order to achieve the well-compatibility in polymeric structure. Moreover, the adhered PD can act as the anchor to graft the secondary functional biopolymers by the thiols, imino and amines which consequently leads to development of innovative hydrogels with admire properties (Cheng et al., 2012; Cheng et al., 2013; Xing et al., 2017). However, according to our knowledge, the role of PD-functionalized GO to develop shear thinning hydrogel has never been investigated.

Herein, we developed a novel injectable shear-thinning and mechanically robust hydrogel based on κ-CA-GO for soft tissue engineering. In this respect, dual-crosslinkable KaMA was primary synthesized to create photo- crosslinkable hydrogels emphasizing their use in the context of tissue engineering. Subsequently, KaMA-GO hybrid hydrogels, consisting of various amounts of GO nanosheets (1, 4, 10 and 20 wt.%) were developed. In order to provide a robust and shear-thinning hydrogel, GO nanosheets were primarily functionalized with a thin layer of PD (GOPD). It is expected that the proposed shear-thinning and mechanically robust hydrogel can be used for soft tissue engineering.

2. Materials and methods

2.1. Materials

Kappa-Carrageenan (κ-CA, sulfated plant polysaccharide), a linear polysaccharide constructed of repeated 1,3-linked β-D-galactopyranose and 1,4-linked 3,6-anhydro-D-galactopyranose units (14.57 wt.% K^+, 5.50 wt.% Ca^{2+} tested by ICP, $M_W = 3 \times 10^5$ g/mol) was purchased from Sigma-Aldrich. The 3,6-AnGal/Gal ratio was investigated about 1:1.03 (Navarro & Stortz, 2003). Moreover, methacrylic anhydride (MA) ($C_8H_{10}O_3$) (Sigma-Aldrich, 64100), photoinitiator (PI) Irgacure D-2959 (2-Hydroxy-4′-(2-hydroxyethoxy)-2-methylpropiophenone) ($C_{12}H_{16}O_4$) (Sigma-Aldrich, 410896), potassium chloride (KCl, Merck) and sodium hydroxide (NaOH, Merck Co) were purchased to synthesize dual-crosslinkable KaMA. Dialysis membrane (Mol. Wt. cut-off ~12–14 kDa) was obtained from Betagen Co, Mashhad, Iran. Graphene oxide (GO) powder (purity > 99%, thickness: 3.4–7 nm, 6–10 layers, Nanosany Co, Mashhad, Iran), methanol (CH_3OH, Merck Co), acetic acid (CH_3COOH, Merck Co), dopamine (DA) ($C_8H_{11}NO_2$, Merck Co), ammonium persulfate (APS, Merck Co), trisaminomethane (Tris, Merck Co), hydrochloric acid (HCl, Merck Co) were provided to synthesize polydopamine (PD) coated GO (GOPD). Moreover, double distilled water (DDW) was used at all experiments.

2.2. Synthesis of Kappa-carrageenan methacrylate (KaMA)

Methacrylation of κ-CA was carried out by reacting κ-CA with MA, fallowing the recent study, conducted by Mihaila et al. (2013). The chemical interaction is provided in Supplementary Fig. S1. Briefly, in order to reach homogeneous 1 wt.% solution, κ-CA was fully dissolved in 100 ml DDW at 50 °C. Consequently, 4.2 ml MA was added to solution and allowed to react for 6 h at 50 °C. To adjust the pH (~8.0), 5 M NaOH solution was added drop-wise. After 6 h, the resulting κ-CA solution was dialyzed against DDW using 12–14 kDa cutoff cellulose dialysis membrane for 7 days at 4 °C to remove excess of unreacted MA as well as by-products formed during the reaction. Refined KaMA solution were frozen at −80 °C and then lyophilized. Until further use, the lyophilized KaMA was stored at −20 °C, while it was protected from light.

2.3. Synthesis of dopamine functionalized GO (GOPD) nanoparticles

Dopamine functionalized GO (GOPD) nanoparticles were prepared by the self-polymerization of dopamine as a coating layer on the GO nanoparticles based on previous studies (Tan, Liu, & Ren, 2017). After dispersion of 20 mg GO nanosheets in 50 ml DDW for 30 min, 3 mg APS, 25 mg DA and 5 ml Tris-HCl solution (200 mM, pH 8.5) were added to it, consequently. The resulted suspension was endured a polymerization reaction at room temperature for 2 h to synthesize GOPD nanoparticles. The resulting GOPD nanoparticles was removed, and sufficiently rinsed with a methanol: acetic acid solution (volume ratio = 9:1) using centrifugation at 3500 rpm for 10 min. Finally, the remained precipitate was dried under vacuum for 24 h.

2.4. Synthesize of KaMA-GOPD hybrid hydrogel

KaMA-GOPD hybrid hydrogels consisting of various concentrations

of GOPD (1, 4, 10 and 20 wt.%) were prepared. Primarily, prepolymer of freeze dried KaMA solution in DDW water with concentrations of 1.5 wt.% was prepared at 80 °C. Consequently, specific amounts of GOPD were added. Afterward, 0.5 wt.% PI solution in acetone was added to KaMA-GOPD solution and let it to fully mixed, while they protected from light. Consequently, 2 ml of KaMA-GOPD solution was added into disc-shaped polystyrene molds (10 mm diameter and 20 mm height) followed by gently adding a 5 wt.% KCl solution to initiate physical crosslinking. After 20 min, the samples were removed from the molds and washed in DDW in order to remove the salt residues. Finally, ion-crosslinked KaMA-GOPD hydrogels were chemically crosslinked by 180-sec irradiation of UV-A (1.69 mW/cm^2). Depending on the concentrations of GOPD nanoparticles (1, 4, 10 and 20 wt.%) in the hybrid hydrogels, the samples were named K-G1, K-G4, K-G10, K-G20, respectively. KaMA hydrogel was also similarly fabricated as the control. In this regard, after preparation of 1.5 wt.% KaMA solution in DDW water at 80 °C, 0.5 wt.% PI solution in acetone was added to it. Consequently, the two-step process of ionic crosslinking in 5 wt.% KCl solution followed by chemical crosslinking in 180-sec irradiation of UV-A was performed.

2.5. Characterization of KaMA-GOPD hybrid hydrogel

The microstructure of hydrogels was evaluated using a Scanning Electron Microscopy (SEM, Philips, XL30). The samples were drowned in liquid nitrogen, followed by freeze drying for 24 h. Before imaging, the samples were sputter coated with a thin layer of gold using a Hummer 6.2 sputter. Moreover, the pore size distribution of hydrogels (n = 30) was achieved using ImageJ software, based on the SEM images. Moreover, the thickness (n = 3) and surface topography of GOPD were investigated using atomic force microscopy (AFM, Veeco, CP II, PCResearch, USA). After preparation of GO and GOPD suspensions in DDW (0.1 mg/ml) using an ultrasonic oscillator (20 kHz, 50 W) for 30 min, they were coated on a Si wafer using a spin-coater (Modern Technology Development Institute, Iran) at the optimized rate of 500 rpm for 5 min. In order to study the surface modification of GO nanosheets with dopamine, X-ray diffraction (XRD, X'Pert Pro X-ray diffractometer, Phillips, Netherlands), Fourier transform infrared spectroscopy (Tensor27, Bruker, Germany) and Raman spectroscopy (Takram P50C0R10, 532 nm, Iran) were performed. Furthermore, the absorption spectra were measured using a UV–vis spectrophotometer (EU-2800DS, Onlab, China)

The chemical modification of κ-CA was determined by H NMR spectroscopy (Bruker Avance II, 500 MHz). In this regard, H NMR spectra of κ-CA and KaMA were collected in D_2O at 25 °C, at a frequency of 500 MHz on a Varian INOVA NMR spectrometer with a single axis gradient inverse probe. Moreover, the chemical composition of the resultant KaMA-GOPD hybrid hydrogels was verified by Fourier transform infrared spectroscopy (Tensor27, Bruker, Germany), in the range of 500–4000 cm^{-1}.

2.6. In vitro physiological stability evaluation of KaMA-GOPD hybrid hydrogel

To study the effect of GOPD content on the equilibrium water content (EWC) and stability of the hydrogels, KaMA-GOPD hydrogels (n = 3) consisting of various amounts of GOPD nanoparticles were lyophilized, weighted (W1) and, subsequently, soaked in phosphate buffer solution (PBS) at 37 °C for 1 h. It needs to mention that PBS was prepared according to previous protocols (Popuri, Harris-Logie, Lino, Cadogan, & Lee, 2014). After being wiped off to remove the excess liquid from the samples surface, the wet hydrogels were weighted (W_2) and the EWC was measured according to Eq. (1) (Mihaila et al., 2013):

$$EWC = \frac{(W_2 - W_1)}{W_2} \times 100 \quad (1)$$

To study the degradation rate of hydrogel, the samples (n = 3) were lyophilized and weighed (W_1), prior to incubation in 37 °C. After 3, 24, 48 and 72 h of incubation, the specimens were lyophilized again and were consequently weighed (W_2). Finally, the weight loss of hybrid hydrogels was calculated according to Eq. (2) (Lokhande et al., 2018):

$$Weight \quad loss\ (\%) = \frac{(W_1 - W_2)}{W_1} \times 100 \quad (2)$$

2.7. Rheological properties of KaMA-GOPD hybrid hydrogel

All rheological measurements were carried out on a MCR 502 (Anton Paar, Germany) rheometer equipped with 25 mm parallel plate geometry at a gap of 500 μm. Primarily, flow test was achieved to assess the viscosity of polymer solution while shear rate was modulated from 0.01–100 s^{-1} at 37 °C. Subsequently, oscillatory stress sweep was applied between 0.1–1000 Pa at 37 °C and at a frequency of 0.1 Hz. All these tests were performed for both KaMA and KaMA-GOPD (K-G4), pre-polymer solution and crosslinked hydrogels, to investigate the effect of GOPD nanoparticles on rheological and injectability of pre-polymer solution, and viscoelastic behavior of crosslinked hydrogels.

2.8. Compressive mechanical analysis of KaMA-GOPD hybrid hydrogel

Mechanical properties of KaMA-GOPD hydrogels were determined using a tensile tester (Hounsfield H25KS, United Kingdom) with a load cell capacity of 500 N. Before compressive mechanical testing, the cylinders of specimens with diameter of 10 mm and thickness of 20 mm (n = 5) were dually crosslinked, according to the previous protocol. The samples were compressed with a strain rate of 1 mm/min up to 60% strain. Compressive modulus and strength (at 60% strain) were calculated for each composition. Compressive modulus was defined as the slope of the linear region of the strain/stress curve, corresponding to 5–15% strain. Furthermore, cyclic compressive tests were performed at a rate of 0.5 mm/min until 60% of strain, as 1st complete loading-unloading cycle. Then, the specimens were put in PBS solution for 2 h and 2nd cycle was applied. The energy lost during the cycle was also calculated by determining the area between the loading and unloading cycle of curves. Finally, the sample's recovery was estimated based on comparison between 1st and 2nd loading curves, based on Mahalia et al. researches (Mihaila et al., 2013). Finally, in some hydrogels, work-hardening energy was determined by measuring area between 1st and 2nd loading curves, after 2nd loading curve crossed 1st loading curve.

2.9. Cell culture

In order to evaluate the role of GOPD nanoparticles on the cellular behavior of KaMA hydrogel, L929 fibroblast cell line, purchased from Royan Institute of Iran, was applied. First, disk-like hydrogels with 10 mm diameter and thickness of 1 mm were prepared. Before cell seeding, the specimens were washed with phosphate buffer saline (PBS, Bioidea, Iran), sterilized for 30 min in 70% (v/v) ethanol and 2 h under UV light. Fibroblast cells were cultured in Dulbecco's Modified Eagle Medium (DMEM-low, Bioidea, Iran) containing 10%(v/v) fetal bovine serum (FBS, Bioidea, Iran) and 1%(v/v) streptomycin/penicillin (Bioidea, Iran) in incubator at 37 °C containing 5% CO_2. Consequently, fibroblast cells with a density of 10^4 cells/well were seeded on the hydrogels and tissue culture plate (TCP) (control). Finally, the cell-seeded hydrogels were incubated at 37 °C under 5% CO_2 for 5 days, while culture medium was changed after 3 days.

2.9.1. Cell viability study

To evaluate the viability of fibroblasts seeded on hybrid hydrogels, after 1, 3 and 5 days, calcein-AM/ ethidium homodimer (EthD-III) live/dead assay (Biotium, UK) was performed. After rinsing the cell-cultured samples, 100 μl of live/dead solution consisting of 2 μM calcein AM and

4 μM ethidium homodimer was added to the samples to cover the cell monolayer, and incubated for 1 h at 37 °C. The samples were then imaged using an inverted fluorescence microscope (Nikon TE2000-U, Japan). Finally, the cell viability was determined using Image J software by the number of live cells (green cells) divided by total cell number (green and red stain) (n = 3).

2.9.2. Immunostaining for cell cytoskeletal organization

In order to assess the role of GOPD on the cytoskeletal organization (F-actin) of fibroblast seeded on the various hydrogels, DAPI/phalloidin staining was performed. The cell-seeded samples were fixed using 4%(v/v) paraformaldehyde (Sigma Aldrich Co, USA) for 2 h. Then, the cells were permeabilized in 0.1%(v/v) Triton X-100 (Sigma Aldrich Co, USA) for 5 min, fallowing incubation with 2%(v/v) bovine serum albumin (Sigma Aldrich Co, USA) in PBS for 1 h in order to decrease nonspecific background staining. Therefore, after triple rinsing with PBS, fibroblast cells were incubated with 1:1000 dilution of 40, 6-diamidino-2-phenyl indole dihydrochloride (DAPI, sigma-Aldrich, Germany) in PBS for 5 min to stain cell's nuclei. Subsequently, the actin filaments were stained with 1:40 dilution of rhodamine phalloidin (cytoskeleton, USA) solution for 30 min. Finally, the stained samples were studied using a fluorescence microscope (Nikon TE 2000-U, Nikon instruments Inc., USA). Moreover, to quantify cell proliferation, cell area of each sample (n = 3), were assessed.

2.9.3. Cell survival study

The relative cell proliferation was investigated using MTT assay, performed according to the manufacturer protocol (Sigma Aldrich Co, USA). At the specific time points (1, 3 and 5 days), the culture medium was discarded and 300 μl MTT solution (0.5 gr/ml) was added to the cell-seeded samples and control. After 3 h incubation at 37 °C under 5% CO_2, the dark blue formazan crystals were dissolved in DMSO (Merck, Germany) and were kept for 30 min at 37 °C. Subsequently, 100 μl dissolved formazan solution of each sample was moved to 96-well plate and the optical density (OD) of each well was measured with a microplate reader (Biotek Instruments, China) against DMSO (blank) at a wavelength of 490 nm. The relative cell survival (% control) was calculated based on the following Eq. (3) (Mokhtari, Ghasemi, Kharaziha, Karimzadeh, & Alihosseini, 2018):

$$\text{Relative cell survival (\% control)}: \frac{X_{Sample} - X_b}{X_c - X_b} \quad (3)$$

Where X_{Sample}, X_b and X_c were absorbance of the sample, blank (DMSO) and control (TCP), respectively.

2.10. Statistical analysis

The data in this study was analyzed using one-way ANOVA analyses. To determine a statistical significance between groups, Tukey–Kramer post-hoc test using GraphPad Prism Software (V.6) was applied and P-value < 0.05 was defined as statistically significant.

3. Results and discussion

3.1. Characterization of GOPD nanosheets

In this study, we offered a robust and shear-thinning KaMA-GOPD hydrogel based on muscle-inspired adhesion mechanism as well as nanohybrid formation strategy for soft tissue engineering. This nanohybrid hydrogel was prepared via a two-step process: synthesize of GOPD nanosheets and consequently nanohybrid formation. According to Fig. 1A, dopamine was firstly intercalated in to the GO nanosheets with free catechol and amino groups and in-situ oxidized in the alkaline environment leading to the formation of a thin PD layer. Amino is the functional group that attached the PD layers to GO surfaces. This interaction led to enhanced number of catechol groups on the nanoparticles allowed the anchor-like PD to connect with other chemical structures via hydrogen bonding, π–π stacking interactions, physical entanglement, chemical crosslinking and even non-covalent bonding which might lead to superior mechanical and physical characteristics (Gaharwar et al., 2010; Phua et al., 2012; Xu, Yang, Neoh, Kang, & Fu, 2010). In addition, PD layer could significantly affect the morphology and size distribution of GO nanoparticles. SEM and AFM techniques were used to study the surface topography of both GO and GOPD nanoparticles. According to the SEM images of GO and GOPD (Fig. 1B), the GO surface was completely covered by a thin layer of coating, after PD coating. The GO nanosheets consisted of a smooth surface, while GOPD became rough after PD coating, which was similar to other results (Su et al., 2018). Moreover, the agglomeration of GO nanosheets originated from π-π-stacking interactions was significantly reduced. Besides, nanoparticles were characterized by AFM (Fig. 1C and D) in order to evaluate the thickness of nanoparticle's sheets, before and after PD coating process. The results revealed the enhanced surface roughness, confirming the SEM images on the GO covered PD layer. Furthermore, the average thickness of GO nanosheets was estimated about 11.7 nm (Fig. 1C), due to the functional groups on the GO surfaces, which was much thicker than pristine graphene (Yamaguchi, Eda, Mattevi, Kim, & Chhowalla, 2010). That was also a big number for GO thickness, showing that nanoparticles were agglomerated and not fully dispersed in water. Instead, the average thickness of GOPD was 24 nm (Fig. 1C), showing enhanced thickness compared to GO nanosheets (about 12 nm), demonstrating that PD layer was successfully added to GO. This result was similarly reported in other researches (Hwang, Kang, Ruoff, Shin, & Park, 2014; Mu et al., 2015).

In addition, oxidization of DA to PD could reduce GO without employment of toxic reductants such as hydrazine which are not biocompatible. According to Fig. 1E, the color of the GO solution (0.1 mg/ml) was changed from brownish to dark grey, demonstrating the successful reduction of GO, that was similar to other researches (Jing, Mi, Napiwocki, Peng, & Turng, 2017; Liu et al., 2012). The successful surface functionalization of GO using PD and reduction of GO was studied by UV–vis spectroscopy. Fig. 1F shows the UV–vis spectra of GO and GOPD dispersed in DDW. The GO spectrum consisted of a specific absorption peak at 224 nm due to the $\pi \rightarrow \pi^*$ transition of aromatic C═C bonds, as similarly reported previously (Xu et al., 2017). After functionalization with PD, this peak shifted to 294 nm, confirming the successful reduction of GO during polymerization of DA to modify GOPD (Jing et al., 2016). Moreover, we observed that absorbance of GOPD in the visible range increased compared to GO. Fu, Lai, Jia, and Yu (2014) reached the same results, and suggested that the dispersion of functionalized-GO did not show any perceptible precipitation, implying that the PD layer was a great stabilizer to prevent the stacking of the reduced graphene sheets. FTIR spectrum of GOPD also similarly confirmed the reduction of GO after coating with PD (Fig. 1G).

The FTIR spectrum of dopamine consisted of a C—C bond at 826 cm^{-1}, C—H bond at 1291 cm^{-1}, C—C bond of the aromatic ring at 1510 cm^{-1} and a bending vibration of the amine group at 1605 cm^{-1}. Moreover, the stretching vibrations of C—H revealed at 3040 cm^{-1}, while the stretching vibration of the hydroxyl group of catechol and stretching of the amine group was observed at 3320 cm^{-1} and 3340 cm^{-1}, respectively (Fu et al., 2014; Liu et al., 2012; Ma, Niu, Zhang, & Cai, 2011; Zhu et al., 2017). The spectrum of GO nanosheets consisted of multiple peaks in the range of 900 to 1500 cm^{-1}, which could be assigned to the various functional groups, such as C—O at 1060 cm^{-1}, C—O—C at 1250 cm^{-1}, C—OH (stretching) at 1398 cm^{-1}, C═O (stretching vibration) at 1620 cm^{-1} and C═O in carboxylic acid at 1730 cm^{-1} (Fu et al., 2014; Liu et al., 2012; Marcano et al., 2010). After modification of GOPD, the intensity of GO's peaks decreased, corresponded to reducing the amount of oxygen containing groups at the surface of GO. Our results confirmed the successful reduction of the GO nanosheets after dopamine functionalization. In this regard, the peak belonging to the carboxyl group in GOPD and the peak intensity

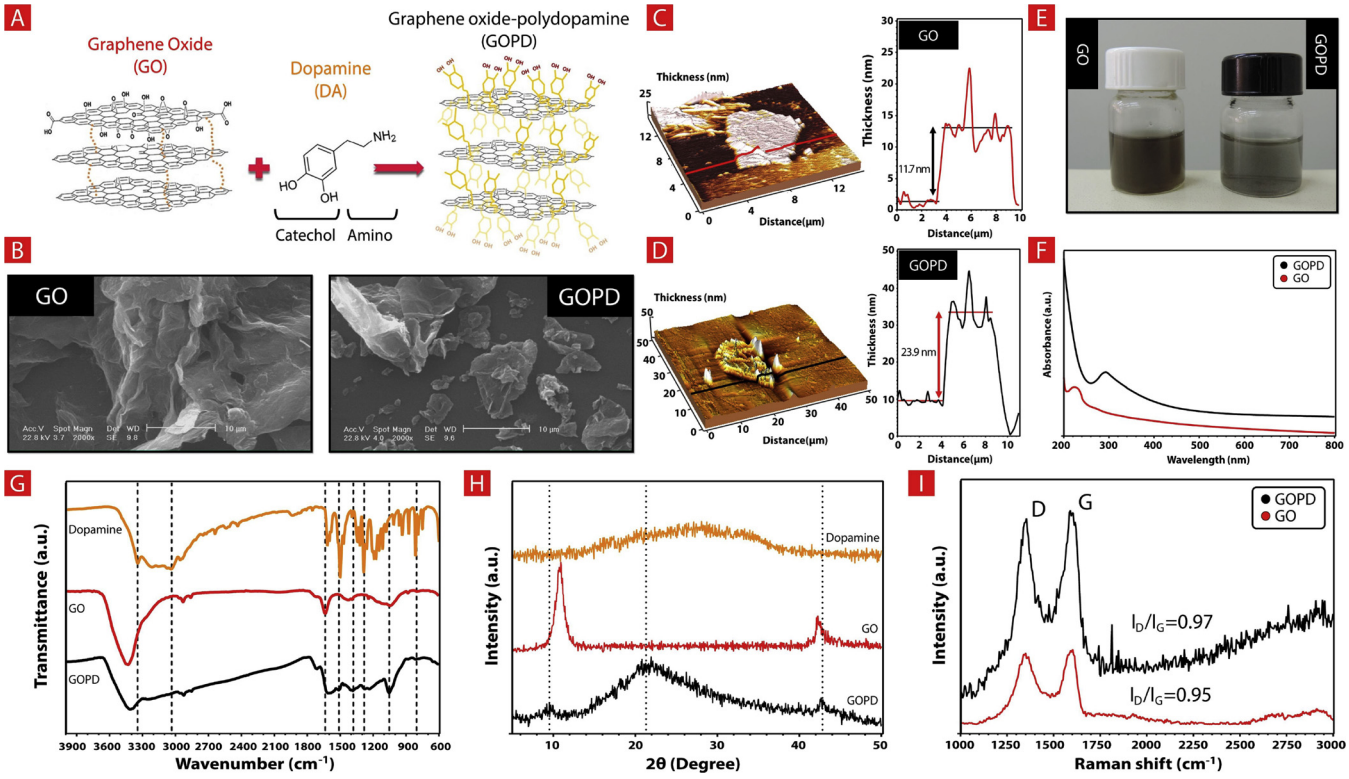

Fig. 1. Characterization of GOPD: A) The schematic representation of the formation of GOPD nanosheets. B) SEM images, of GO and GOPD nanoparticles. AFM image and height profile of C) GO and D) GOPD. E) The representative suspensions of GO and GOPD in water. The change in the color of suspension from brown to dark grey confirmed the reduction of GO after formation of GOPD. F) UV–vis absorption spectra of GO and GOPD. G) FTIR spectra and H) XRD patterns of dopamine, GO and GOPD. I) Raman spectra of GO and GOPD.

between 900 and 1400 cm^{-1} decreased, significantly. Additionally, the specific absorbance bands of dopamine were disappeared in GOPD confirming the effective polymerization of dopamine. Furthermore, the broad bands at the range of 900 to 1800 cm^{-1} with no distinguishable peaks, representing the highly complex structure of PD was also observed, as similarly reported in other researches (Xiong et al., 2014; Zangmeister, Morris, & Tarlov, 2013). Additionally, FTIR spectrum of the GOPD exhibited new peaks at 1358 cm^{-1} and 1504 cm^{-1}, due to the stretching vibration of C—N—C of indole ring and the N—H bending mode of aromatic secondary amine in GOPD, respectively. These peaks confirmed the successful polymerization of dopamine, which was consistent with other researches (Centeno & Shamir, 2008). Additionally, the presence of the board peak of O—H group in the GO nanosheets at 3450 cm^{-1} was often due to absorbed humidity which could not be avoided. Based on our result, DA have been used as a reducing agent, as the oxygen groups on the surface of GO were chemically reduced during the polymerization process. To further assess the reduction of GO and interaction between PD and GO, XRD patterns were studied (Fig. 1H). Dopamine consisted of a low intensity and board pick between $2\theta = 13–38^{\circ}$ due to its amorphous structure. In another word, XRD pattern of GO consisted of the characteristic peaks of GO centered at $2\theta = 10.5^{\circ}$ and 42.4° corresponding to the d-spacing of 0.85 and 0.23 nm, respectively, due to the formation of hydroxyl, epoxy and carboxyl groups, respectively. In contrast to GO, the GOPD revealed the small and broad peak at $2\theta = 9.7^{\circ}$ with *d*-spacing of 0.92 nm, indicating that most of the oxygen functional groups of GO was efficiently attacked by the polymerization reaction of dopamine and GO nanosheets (Xu et al., 2010). Moreover, it could be concluded that the incorporation of dopamine onto the GO nanosheets and in-situ polymerization enlarged the *d*-spacing of GO nanosheets. The other peak at around $2\theta = 21.5^{\circ}$ was corresponded to the *d*-spacing of 0.44 nm, belonging to the partial reduction of GO by polymerization of dopamine (Fu et al., 2014). Moreover, it could be due to the attached dopamine on the GO nanosheets, since the same broad peak was detected in the XRD pattern of pure dopamine.

Raman spectroscopy was also applied to characterize the GOPD nanoparticle, particularly for distinguishing ordered and disordered crystal structures of carbon (Fig. 1I). The peak at around 1597 cm^{-1} (G band) was corresponded to the vibration of the sp^2-bonded carbon atoms in a two-dimensional hexagonal lattice, while a peak at about 1325 cm^{-1} (D band) was an indication of disorder in the Raman of the GO. The disorder in the GO nanosheets was originated from defects associated with vacancies, grain boundaries and amorphous carbon species (Ferrari et al., 2006; Schönfelder et al., 2007). Our results demonstrated that, the D band of GOPD remained unchanged, when compared to that of GO, while the G band of GOPD was shifted to 1585 cm^{-1}, confirming the successful reduction of GO to GOPD (Zheng et al., 2012). Furthermore, the intensity ratio of the D to G band (I_D/I_G) was calculated, reflecting the graphitization degree of carbonaceous materials and the defect density (Zhao et al., 2010). Our findings showed that I_D/I_G of GO was about 0.95 which enhanced to 0.97, due to a decrease in the average size of the sp^2domains upon reduction of GO (Fang et al., 2017). It could also be due to the formation of defects by the elimination of oxide functional groups attached to the GO surface (Eigler, Dotzer, & Hirsch, 2012). After functionalization with PD, the G band was also broadened and shifted to 1601 cm^{-1}, whereas the intensity of the D band at 1325 cm^{-1} increased, substantially. These results confirmed the semi-reduction of GO and successful polymerization of dopamine leading to an effective development of GOPD. Ye et al. (2014) also found these changes, because of a decrease in the size of the in-plane sp^2 domains and a partially ordered crystal structure of graphene.

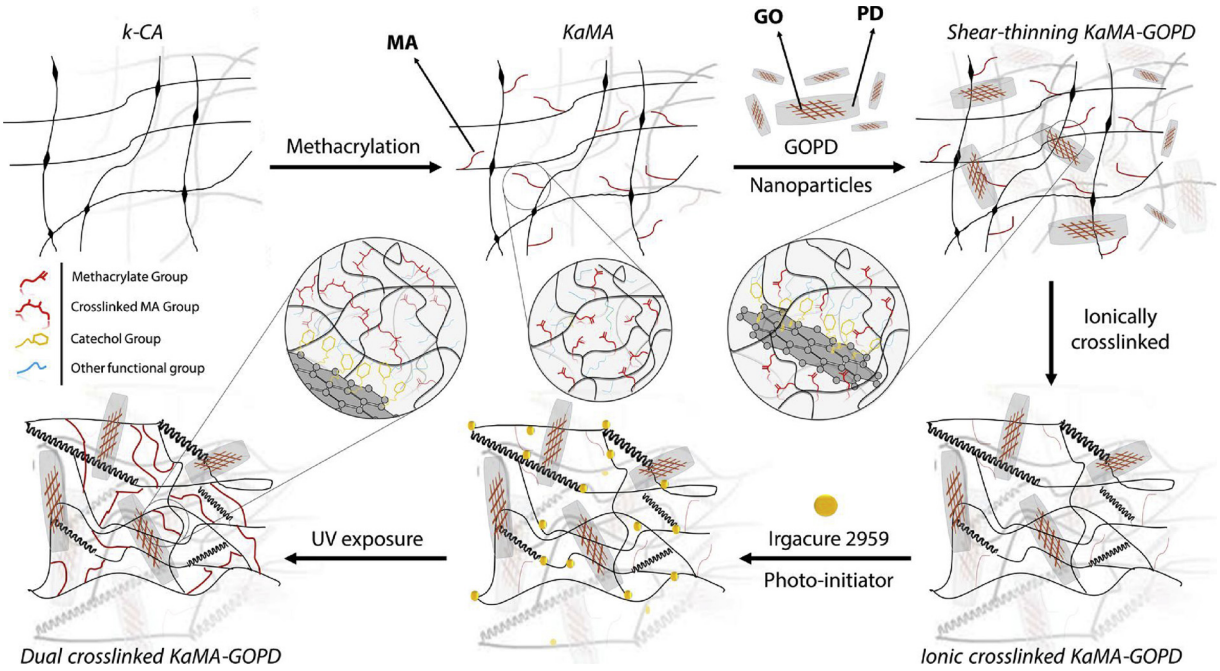

Fig. 2. Schematic outlining the design strategy to synthesize nanohybrid KaMA-GOPD hydrogels.

3.2. Characterization of nanohybrid KaMA-GOPD hydrogel

After synthesize of GOPD, methacrylation process was completely accomplished (Supplementary Fig. S1). Subsequently nanohybrid KaMA-GOPD hydrogels were developed, according to Fig. 2. KaMA is a photocrosslinkable polymer which structurally mimic glycosaminoglycan component of native ECM. UV-crosslinkable KaMA has recently been proposed for tissue engineering applications (Mihaila et al., 2013; Thakur et al., 2016). However, we incorporated GOPD within KaMA hydrogel in order to develop shear-thinning and robust hydrogel for soft tissue engineering. It was expected that the chemical interaction between catechol groups of PD with other moieties on KaMA might be provided leading to improvement of the KaMA hydrogel properties.

At first, the successful methacrylation process of κ-CA was investigated using H NMR spectroscopy (Fig. 3A). H NMR spectrum of κ-CA spectrum consisted of the following chemical shifts: H NMR δ = 4.97 (H1), δ = 3.95–4.06 (H4), δ = 3.73–3.80 (H3), δ = 3.62 (H5, H6) and δ = 3.42 (H2), which were in agreement with other researches (Abad et al., 2011; Campo et al., 2009; Mobarak, Ramli, Ahmad, & Rahman, 2012). After methacrylation process, H NMR spectrum of KaMA consisted of one peak corresponding to the methyl group and double-peaks to vinyl group of the methacrylate group at δ = 1.9–2 and 5.5–6 ppm, respectively; this result confirming the methacrylation of κ-CA. Consequently, nanohybrid hydrogels containing various amounts of GOPD were developed, via two-step ionic and subsequently UV crosslinking process. When KCl was injected, the coil-helix conformational transition occurred rapidly (less than 1 min) leading to the formation of a robust hydrogel. Subsequently, in order to improve mechanical properties, chemically crosslinking was performed via UV-crosslinking process. Fig. 3B represents the image of nanohybrid hydrogels consisting of various amounts of GOPD. The color of samples changed from white (KaMA) to completely black (K-G20) as a result of GOPD incorporation.

ATR-FTIR spectroscopy was applied in order to investigate the formation of nanohybrid hydrogels of KaMA-GOPD (Fig. 3C). The spectrum of κ-CA consisted of some main characteristic peaks including a sharp vibration of a sulfated group C—O—S bond, vibration of C—C, stretching O═S═O and stretching vibration of O═S═O at 820, 925, 1010 and 1210 cm^{-1}, respectively (Lokhande et al., 2018; Mihaila et al., 2013; Thakur et al., 2016). The validity of methacrylation procedure of κ-CA at KaMA was further confirmed by the main peaks of C—C at 1530 cm^{-1}, C═C at 1620 cm^{-1} and carbonyl (C═O) at 1730 cm^{-1} which were not appeared in κ-CA. Moreover, the sulphate groups of κ-CA was shifted slightly in the KaMA spectrum at 1215 cm^{-1} (O═S═O antisymmetric vibration) and 1023 cm^{-1} (O═S═O symmetric bond), respectively. This result showed that the essential sulphate group of κ-CA, playing an important role in ionic crosslinking, was not affected by the methacrylation reaction conditions.

The presence of GOPD within the dual crosslinked KaMA hydrogel was also proved by FTIR spectroscopy (Fig. 3C). With increasing amounts of GOPD in KaMA hydrogel, a new peak at 1358 cm^{-1}, due to the stretching vibration of C—N—C of indole ring, could be detected. Furthermore, the intensity of the peaks at 1530 cm^{-1} (related to C—C band) and 1730 cm^{-1} (related to C═O band) were slightly decreased from K-G1 to K-G20. Moreover, the C═C absorbance band at 1620 cm^{-1} in K-G20 was disappeared confirming that nanoparticles affected the C═C band by interaction with polymer.

In order to investigate the effect of GOPD, nanohybrid hydrogels were also studied by XRD analysis (Fig. 3D). XRD pattern of κ-CA consisted of one board peak at 2θ = 19.6° which was not changed after methacrylation procedure. Moreover, XRD pattern of KaMA exhibited five special peaks at 2θ = 28.5°, 39.8°, 50.1°, 58.1° and 74.2° corresponded to the KCl (JCPDS Card number 41-1476), while all nanohybrid hydrogels consisted of these five peaks, without any comparable difference in their intensities. Moreover, the board peak was appeared in the XRD patterns of all K-G series at 2θ = 22°, which its intensity enhanced with increasing GOPD content up to 20 wt.%. This main peak could be improved by overlapping both peaks related to KaMA and peak around 2θ = 21.5° related to GOPD.

In order to investigate the effect of GOPD on structure and pore size of KaMA hydrogel, nanohybrid hydrogels were also studied by SEM images (Fig. 4A). All samples revealed highly porous networks with interconnected pores. This interconnected porous network could promote the nutrient and waste product transportation and enable efficient cell survival and further proliferation. However, GOPD changed the microstructure of KaMA hydrogel and made the pores bigger. Noticeably, according to Fig. 4B, the average pore size of KaMA (41.3 ± 5.5 μm) enhanced to 117.0 ± 17.0 μm at K-G20 hydrogel.

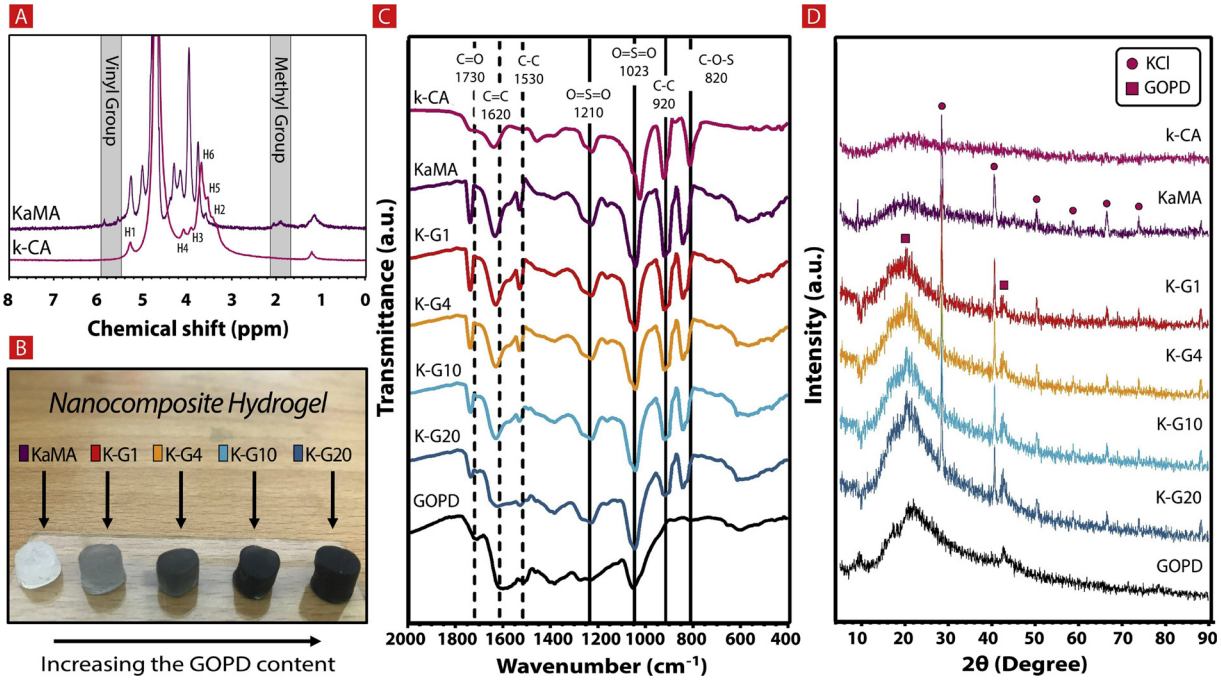

Fig. 3. A) H NMR spectra of κ-CA and KaMA, B) Molded quintet hydrogel, C) ATR-FTIR spectra of κ-CA, GOPD and D) XRD patterns of κ-CA, GOPD and quintet hydrogels.

There was a significant change in pore size between KaMA and all of K-G series, showing that incorporation of GOPD in KaMA resulted in formation of bigger pores. In addition, GOPD nanoparticles with irregular convex-like morphology were distributed in the pore walls of all hybrid hydrogels, as indicated by red arrows. By increasing amount GOPD, these particles transformed to filamentous shape which connected the polymeric wall to each other. High magnification image of K-G20 hydrogel (Fig. 4C) revealed these GOPD nanoparticles which strongly interacted with KaMA structure. In addition, ionic cubes were entrapped between these nanoparticles due to the interaction between catechol group of GOPD and K^+ ions which may affect the degradation and mechanical properties of nanohybrid hydrogels.

3.3. In vitro swelling and degradation properties of KaMA-GOPD hybrid hydrogel

One of the advantages of using hydrogels in soft tissue engineering is their water absorption capability and degradation in biological environment. The swelling ratio and weight loss of the nanohybrid hydrogels are depicted in Fig. 5A,B. Results demonstrated that the presences of GOPD in the hydrogel structures significantly enhanced the swelling ratio of hydrogels (Fig. 5A). Noticeably, swelling ratio of K-G20 hydrogel was 98.8 ± 0.6% which was greater than that of KaMA (95.4 ± 0.2%) which might be due to the hydrophilic nature of GOPD (Jing et al., 2017). GOPD consisted of high density of catechol groups with two hydroxyl groups which facilitated water adsorption during soaking in PBS (Hwang et al., 2014). Moreover, according to the SEM images, pore size of hydrogels enhanced with increasing GOPD content leading to absorption of more water, which confirmed these results. In another study, Huanga et al. (2012) similarly reported that incorporation of graphene-based nanoparticles in hydrogel matrix could promote water uptake.

In order to investigate degradation behavior of hydrogels consisting of different concentrations of GOPD, weight loss of hydrogels during a 72-h period was considered (Fig. 5B). Results indicated that incorporation of GOPD within the KaMA hydrogel reduced the weight loss and degradation rate. KaMA hydrogel revealed a significant weight loss during the first 3 h, and finally, 43 ± 3 wt.% of KaMA was degraded during 72 h. However, increasing the amounts of GOPD dramatically promoted the stability of the nanohybrid hydrogels in biological environment. Noticeably, K-G20 revealed less than 9 ± 2 wt.% weight loss after 72 h immersing in PBS solution. Our findings revealed the interesting fact that, with increasing GOPD content, water holding capability improved, while significantly promoted physiological stability of KaMA- hydrogels. The less stabilization of the KaMA network could be likely due to the exchange of K^+ ions entrapped within the network leading to the weakening of the network. Similar results were reported for various ionically crosslinkable hydrogels such as alginate (Kuo & Ma, 2008), κ-CA (Mihaila, Popa, Reis, Marques, & Gomes, 2014) and gellan gum (Coutinho et al., 2010), In this research, incorporation of GOPD resulted in reduced degradation rate due to the strong interaction between K^+ ions and free catechol groups of PD which resulted in preventing from ion exchange. Similar result was reported for the combination of chitosan with alginate and formation of an electrolytic hydrogel with the ability to protect from ion exchange (Colinet, Dulong, Mocanu, Picton, & Le Cerf, 2010). Moreover, based on Jing et al. study (Jing et al., 2017), the presence of GOPD nanoparticles in hydrogel matrix eventuated in a denser and stronger crosslinking leading to reduced weight loss of hybrid hydrogels.

3.4. Rheological properties of KaMA-GOPD hybrid hydrogel

In order to evaluate the shear-thinning properties of the KaMA-GOPD hydrogels, the rheological properties of K-G4 compared to KaMA hydrogel were investigated. According to Fig. 5C, incorporation of GOPD changed the viscosity of pre-polymer solution which might be due to the electrostatic interactions between catechol group of GOPD and KaMA matrix. It also could be realized that structure stability, moldability and mechanical properties of K-G4 hydrogel were much better than those of KaMA after crosslinking process. In addition, K-G4 sample exposed to stress could restore its first shape, after stress releasing. Finally, the interaction between the catechol groups of GOPD with KaMA enhanced the viscoelastic behavior of cross-linked and overwhelming elastic-like of K-G4 compared to KaMA.

In order to study the effect of GOPD on the shear-thinning characteristics of pre-polymer solution and viscoelastic behavior of

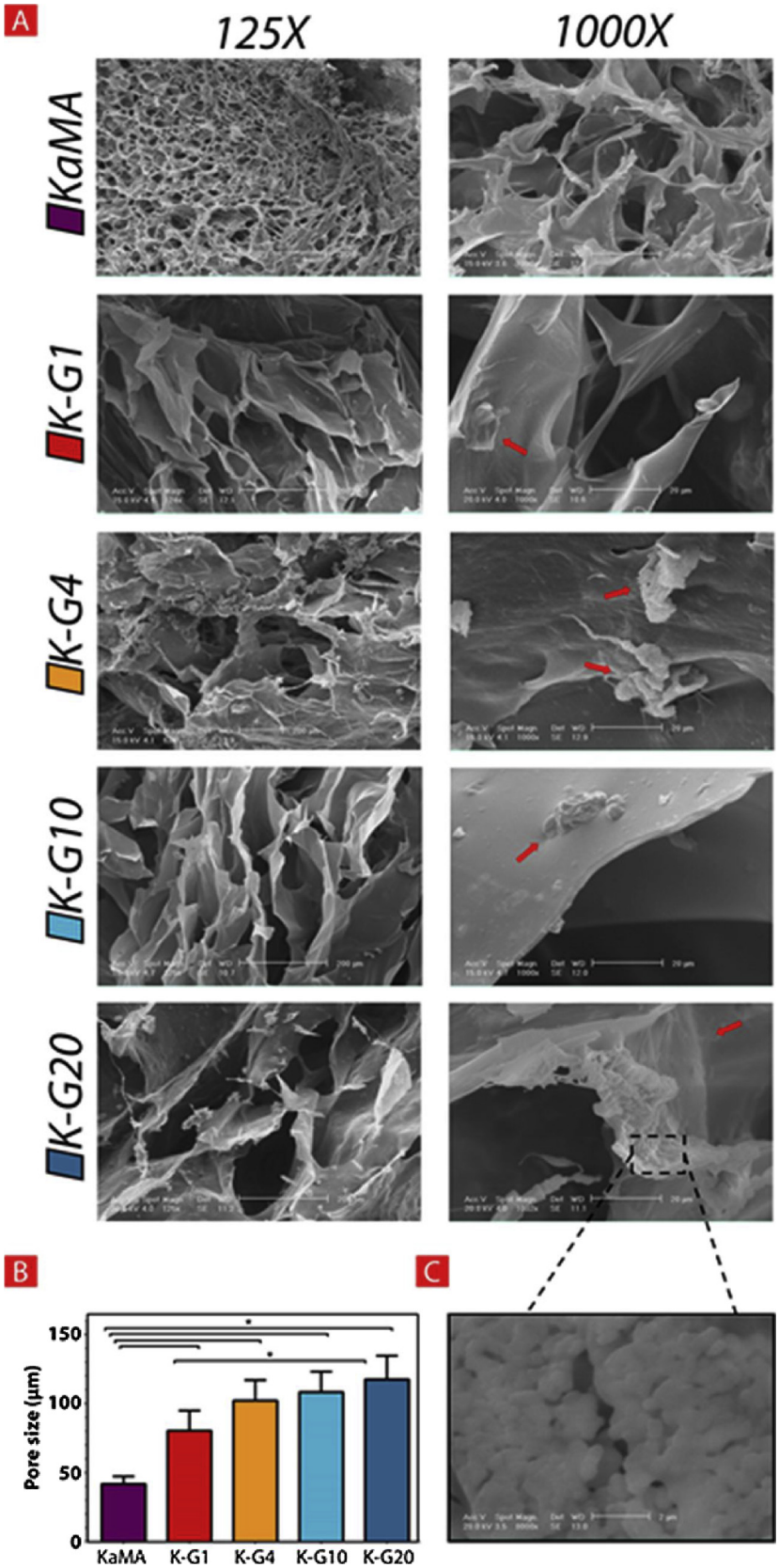

Fig. 4. A) SEM images of the KaMA, K-G1, K-G4, K-G10 and K-G20 hydrogels. B) The average pore size of hydrogels as a function of GOPD content (n = 30) (*: $P < 0.05$). C) SEM image of K-G20 at higher magnification (8000×). (For interpretation of the references to colour in the text, the reader is referred to the web version of this article.)

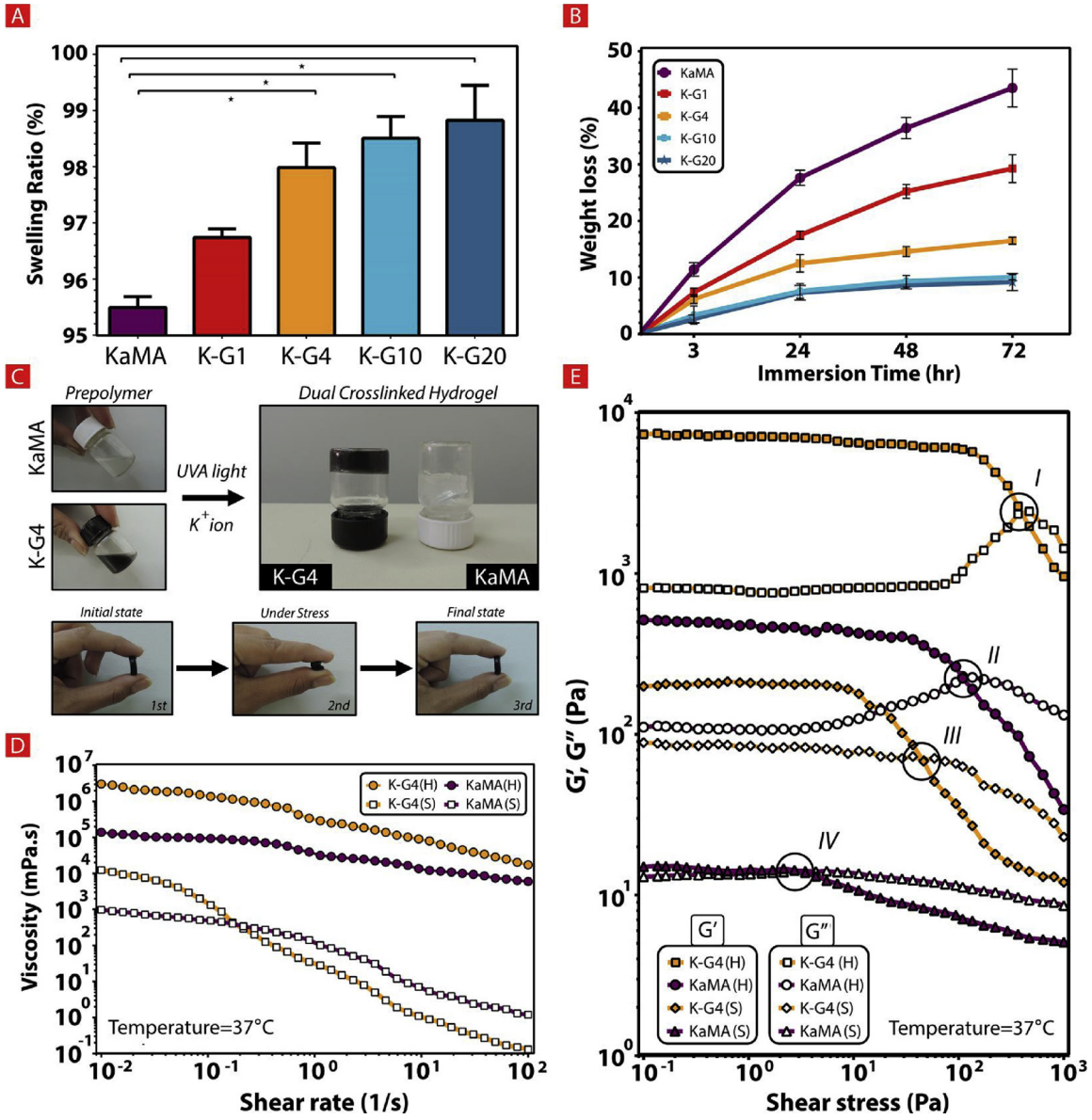

Fig. 5. Physiological stability and rheological properties of KaMA-GOPD hydrogels: A) The equilibrium water content of nanohybrid hydrogels after 1-h soaking in PBS solution at 37 °C (*: $P < 0.05$). B) The weight loss of nanohybrid hydrogels during 72 h-soaking in PBS. C) The effect of GOPD incorporation on the prepolymer solution's viscosity, gelation and viscoelastic behavior of dual-crosslinked hydrogels. D) The viscosity changes of KaMA and K-G4 at both pre-polymer solution (marked with S) and crosslinked hydrogel (marked with H) stages as a function of shear rate (0.01–100 1/s). E) Storage modulus (G') and loss modulus (G'') of KaMA, and K-G4 at both pre-polymer solution (marked with S) and crosslinked hydrogel (marked with S) stages as a function of oscillatory shear stress (0.1–1000 Pa).

crosslinked hydrogels, the viscosity of KaMA and K-G4 pre-polymer solution (marked as S) and crosslinked hydrogel (marked as H) was measured at different shear rates (0.01–100 l/s). Fig. 5D revealed that, at the pre-polymer stage, the viscosity decreased with increasing shear rate for both KaMA and K-G4 compositions. However, incorporation of GOPD in KaMA solution (K-G4 (S)) dramatically improved its shear-thinning behavior. In this regard, when the shear rate increased from 10^{-2} to 10^{2} 1/s, the viscosity of K-G4 (S) decreased from 1.2×10^{4} to 1.3×10^{-1} mPa s. However, the viscosity of KaMA only reduced from 9.7×10^{2} to $1.2 \times 10^{\circ}$ mPa s, in this shear rate range. KaMA-GOPD hydrogel made homogenous structure, though interaction between catechol and other moieties of KaMA (Liang, Zhen, Chen, & Reith, 2009). In this procedure, KaMA selectively attracted the nanoparticles and exhibited dramatic shear-thinning and rapid self-healing behavior which could be promising for tissue engineering application to shield the encapsulated cells from shear mechanical forces (Loebel et al., 2017), Thakur et al. (2016) similarly developed nanosilicate reinforced methacrylate κ-CA and found that the pre-polymer solution showed a viscosity change from 10^{6} to 10^{2} mPa s, when the shear rate increased from 10^{-2} to 10^{2} 1/s. In other work, Lokhande et al. (2018) made 1% κ-CA-2% nanosilicate hydrogel and revealed a decrease in viscosity from 10^{5} to 10^{2} mPa.s, when the shear rate increased from 10^{-1} to 10^{2} 1/s. It seems that in the case of GOPD based nanohybrid hydrogels, electrostatic interactions destroyed, and network broke up, during ruinous shear rate.

Moreover, the elastomeric behavior of KaMA and K-G4 hydrogels was studied. Our results demonstrated that K-G4 hydrogel (K-G4 (H)) revealed greater viscosity than KaMA, at all shear rates. Moreover, the viscosity of the nanohybrid hydrogel reduced slightly with increasing shear rate, confirming the viscoelastic behavior of GOPD incorporated hydrogels. There are some similar results showing considerable interaction between catechol group and K^{+} ions in hydrogels, leading to elastomeric behavior enhancement (Liang et al., 2009). Therefore, superior elastomeric properties of K-G4 compared to KaMA could be due

to the catechol group/K^+ interactions.

The oscillatory shear experiments were performed to analyze rheological behavior of pre-polymer solution and the viscoelastic properties of the hydrogels (Fig. 5E). The storage (G') and loss (G'') modulus are parameters helping to comprehend the viscoelastic properties of hydrogels. In addition, loss factor defined as the ratio between the loss and storage modulus ($\tan\delta = G''/G'$) was similarly measured. It needs to mention that in a loss factor < 1 ($G' > G''$), hydrogels reveal a solid or elastic-like behavior, while a loss factor > 1 ($G' < G''$) resulted in a viscous behavior in hydrogels. In a constant frequency, these parameters measured, while stress swept from 0.1–1000 Pa. With increasing the stress, tan δ enhanced for all samples, until they reached a critical point ($G'' = G'$), that represented a change in the viscoelastic behavior of hydrogels to a liquid-like. This point was highlighted by circles in Fig. 5E. This phenomenon happened, when the crosslinking connection destroyed and consequently the polymeric network of hydrogels was collapsed. At the pre-polymer stage, K-G4 exhibited a higher difference between G' and G'' than KaMA, showing that K-G4 had lower tan δ in the same shear stress, in the initial stage. For instance, in shear stress of 1 Pa, tan δ of K-G4 and KaMA was estimated about 0.40 and 0.93, respectively, revealing the solid-like behavior of K-G4 sample compared to KaMA. Furthermore, in shear stress of 100 Pa, tan δ of K-G4 and KaMA was calculated about 1.97 and 1.38, respectively, confirming the liquid-like behavior of K-G4 in higher shear rates. Moreover, it could be found that at both solid-like and liquid-like zones, K-G4 revealed greater shear-thinning behavior than KaMA. Moreover, while the critical point of K-G4 happened at 46.3 Pa (Circle No. IV), it was occurred at 2.7 Pa (Circle No. III) for KaMA, showing higher stability of nanohybrid hydrogel than KaMA in the same range of shear stress. At the hydrogel state of samples (marked as H), each G' and G' revealed a linear viscoelastic region (0.1–83.4 Pa for K-G4 and 0.1–5.1 Pa for KaMA) representing the stability of hydrogels for both specimens, as similarly reported in previous researches (Mihaila et al., 2013; Yu et al., 2015). Moreover, it was obvious that K-G4 exhibited a longer linear viscoelastic region, showing a stronger structure, reinforced by GOPD which could be deformed at higher stresses. At low stresses for both KaMA and K-G4, the G' value was higher than G''. For example, at 1 Pa, tan δ of K-G4 and KaMA was 0.11 and 0.23, respectively, confirming higher elastic–like behavior of K-G4 at a low stress. At higher stress (for instance, at 100 Pa), tan δ of K-G4 and KaMA was estimated about 0.17 and 1.1, respectively. It was interesting that KaMA went to liquid-like region and its polymeric structure was collapsed at this shear stress, while K-G4 still resisted against failure and preserved its own structure. In addition, the critical point of KaMA (Circle No. II) was at 98.7 Pa, while it was at about 401.4 Pa for K-G4 (Circle No. I). Therefore, it was found that GOPD nanoparticles postponed this point to a higher stress, showing promoted elastic-like behavior of K-G4. In other research, Yu et al. (2015) found out that incorporation of GO to gum resulted in delayed in the critical point to near 11 Pa. In addition, Mihaila et al. (2013) revealed that methacrylation of κ-CA and its chemical crosslinking could promote its critical point to about 250 Pa, while we reached it to higher shear stressed with incorporation of GOPD.

3.5. Compressive mechanical analysis of KaMA-GOPD hybrid hydrogel

The mechanical properties of nanohybrid hydrogels were characterized by applying compression stress-strain test on the dual-crosslinked hydrogels. Fig. 6A revealed that K-G4 hydrogel could preserve its integrity under 80% strain, while KaMA specimen collapsed and could not find its previous state. This behavior was quantitatively evaluated using stress-strain test (Fig. 6B). The comprehensive stress-strain curves were plotted using disk-like samples with diameter of 20 mm and height of 10 mm, up to 60% strain. The plots between 0–20 % strain were also presented with higher magnification. These curves consisted of both elastic and plastic regions, which were dramatically affected by the addition of nanoparticles. Based on the stress-strain curves, the compressive strength, compressive modulus and toughness were evaluated and data are presented in Fig. 6C–E, respectively. In order to investigate the role of dual cross-linking process on the mechanical properties of hydrogels, ionic-crosslinked hydrogels were similarly exposed to the mechanical test and their results are represented in Supplementary Fig. S2. Results revealed that addition of 1 wt.% GOPD to KaMA structure (K-G1 sample) considerably promoted (5.5-folds) the compressive strength of dual-crosslinked KaMA hydrogel from 20.9 ± 2.9 kPa to more than 116.3 ± 9.2 kPa ($P < 0.05$). However, the only significant difference in the compressive strength of K-G series was detected between K-G1 and K-G20 (1.5-folds) ($P < 0.05$). According to Supplementary Fig. S2A, the mechanical strength of ionic crosslinked hydrogels increased gradually from 9.3 ± 3.7 kPa (at KaMA) to 167.3 ± 5.2 kPa (at K-20). Moreover, according to Fig. S2, compared to ionic crosslinked hydrogels, the mechanical strength of dual crosslinked K-G1 and K-G4 hydrogels was significantly improved ($P < 0.05$), confirming the role of chemical crosslinking process to promote mechanical strength. Endorsed mechanical strength of nanohybrid hydrogels might be due to the strong interaction between the catechol groups on the surface of GOPD with other moieties of KaMA and ions, which enhanced with increasing GOPD content. However, incorporation of high amounts of GOPD (e.g. 20 wt.% (K-G20)) led to weakening the methacrylation process noticeably, due to the engagement of methacrylate groups of KaMA with catechol groups of GOPD. Consequently, the difference between mechanical strength of samples was not significant ($P > 0.05$). Moreover, compressive modulus of dual crosslinked hydrogels was significantly enhanced with increasing GOPD content ($P < 0.05$) (Fig. 6D). For instance, the compressive modulus enriched form 12.1 ± 2.2 kPa to 64.7 ± 7.4 kPa for K-G4 (5.4-folds). However, incorporation of 20 wt.% GOPD (K-G20 sample) resulted in reduced compressive modulus to 55.4 ± 5.6 kPa. It was remarkable that by increasing amount of GOPD, the compressive modulus of ionic-crosslinked hydrogels increased gradually (Supplementary Fig. S2B). These data revealed that at lower amounts of GOPD content, the strong interaction between GOPD and KaMA hydrogel resulted in transferring the stress to nanoparticle resulted in enhanced compressive modulus. However, at higher GOPD content, the formation of chemical crosslinking bridges between methacrylate groups of KaMA was prohibited by GOPD leading to reduced compressive modulus from K-G4 to K-G20. Finally, we observed that incorporation of GOPD upon 1 wt.% (K-G1) in the dual-crosslinked hydrogels resulted in the significantly enhanced toughness from 4.0 ± 0.2 kJ/m^3 (for KaMA) to 20.1 ± 0.4 kJ/m^3 (K-G1) (5-folds) ($P < 0.05$), while there was no specific difference between K-G series ($P > 0.05$) (Fig. 6E). Our findings revealed that the maximum toughness was obtained at K-G10 sample (25.3 ± 0.9 kJ/m^3). According to Fig. S2C, the effects of GOPD on the toughness of ionic-crosslinked hydrogels gradually enhanced from KaMA (2.3 ± 0.1 kJ/m^3) to K-G20 (18.2 ± 1.6 kJ/m^3). In addition, the toughness of dual-crosslinked K-G1- K-G10 was considerably higher than that of ionic-crosslinked hydrogels. It could be concluded that chemical crosslinking of the KaMA hydrogel resulted in significantly enhanced mechanical toughness, when GOPD enhanced to 1 wt.%.

In order to study the recovery properties, KaMA-GOPD hydrogels were exposed to the two- cycles of stress-relaxation process. All specimens were compressed until 60% strain with 0.5 mm/min strain rate. Consequently, the specimens were unloaded and the stress was measured. After 2 h soaking in PBS solution, the hydrogels were exposed to one more loading and unloading process. The stress-strain curves of 1^{st} and 2^{nd} cycle and recovery curves are presented in Fig. 7A. According to the stress-strain curves at two cycles, the energy loss at 1^{st} and 2^{nd} cycles were determined by calculating the area between loading and unloading cycles of each curve (Fig. 7B). Our results showed that increasing amount of GOPD concentration improved the surface area under stress-strain curve at 1^{st} cycle. Generally, two factors affect the

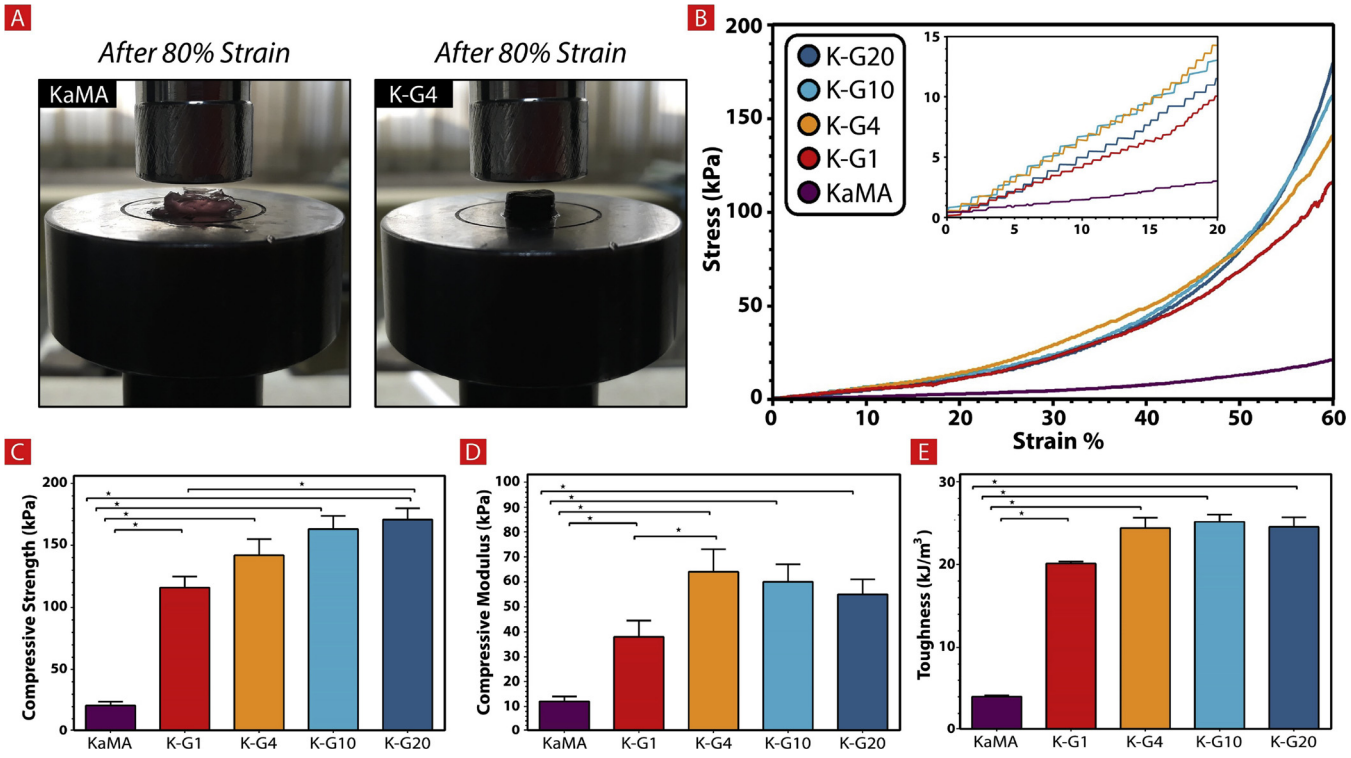

Fig. 6. Mechanical properties of KaMA-GOPD hydrogel: A) Qualitative pictures showing the elastomeric behavior of hydrogels under compressed pressure. B) Stress-strain curves of KaMA, K-G1, K-G4, K-G10 and K-G20 hydrogels. C) Compressive strength (at 60% strain), D) compressive modulus and E) toughness of dual-crosslinked hydrogels (*: $P < 0.05$).

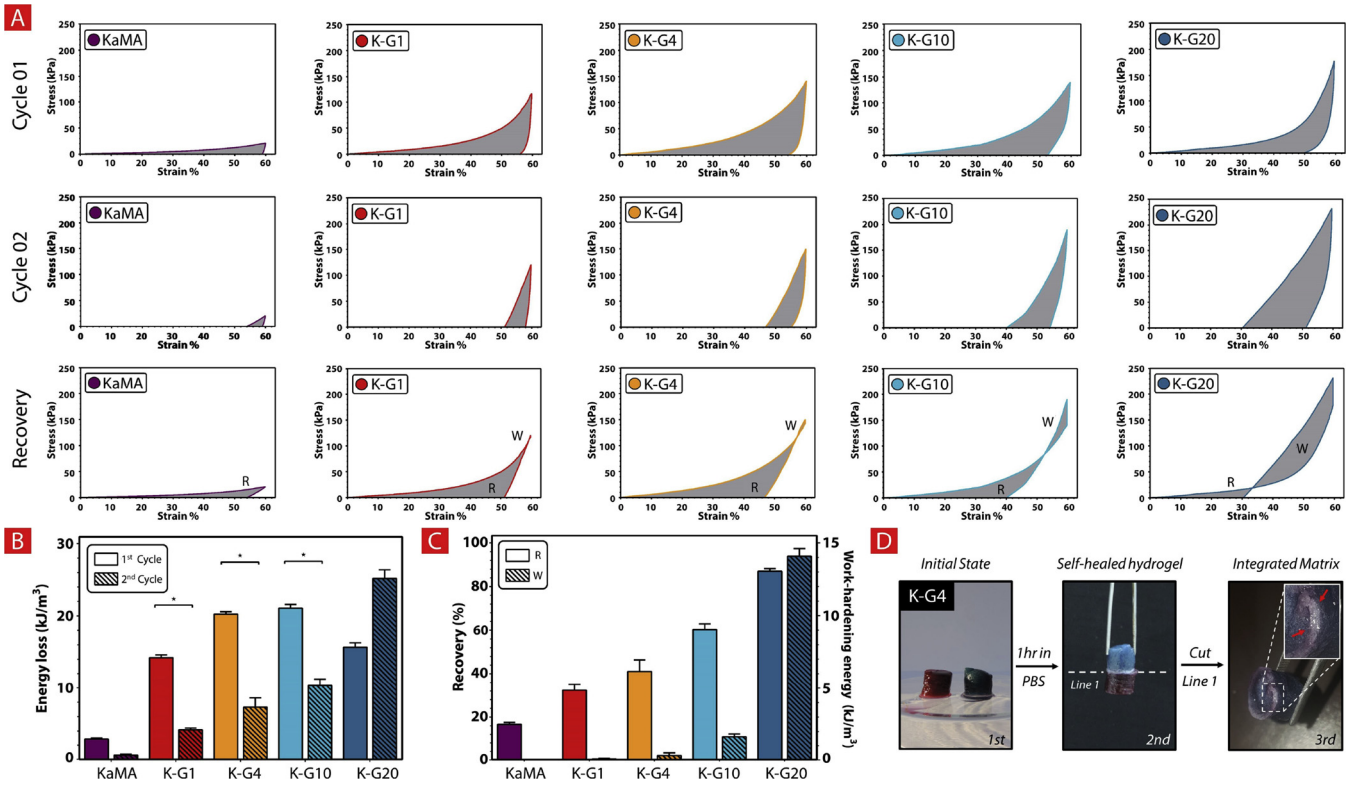

Fig. 7. Compressive properties of KaMA-GOPD hydrogels though cyclic compression test: A) Cyclic stress-strain curves of hydrogels. Hydrogels were compressed until 60% strain, preserved in PBS solution for 2 h and, consequently, compressed for the second cycle. Finally, recovery was evaluated by comparison of area under 1st and 2nd loading curves though the cycle test. B) Energy loss of hydrogels after 1st and 2nd cycles calculated by determining the area between the loading and unloading curves (*: $P < 0.05$). C) Recovery and work-hardening energy of hydrogels though the cyclic test (*: $P < 0.05$). For some hydrogels, work-hardening energy were determined by measuring area between 1st and 2nd loading curves. D) The schematic showing the self-healing properties of K-G4 hydrogels. (For interpretation of the references to colour in the text, the reader is referred to the web version of this article.)

area under stress-strain curves: compressive strength and the strain at the end of unloading cycle. According to Fig. 7B, the ending strain of 1st cycle for KaMA, K-G1 to K-G20 was 58.84, 56.05, 54.31, 52.34 and 49.70%, respectively, showing that the ability of hydrogel matrix to restore initial state after burden catastrophic strain enhanced with increasing GOPD content. KaMA network could absorb energy for mechanical test, while it could not give it back, at the moment. It seems that the interaction between GOPD and KaMA could transfer part of the force to nanoparticle. This phenomenon was due to the effective role of catechol groups of GOPD which created sacrificing bonds with other moieties and K^+ and postponed the destruction of hydrogel leading to better regaining the initial state (Fig. 5C).

For 2nd cycle, after soaking in PBS solution, some of hydrogels such as KaMA absorbed water while others such as K-G10 and K-G20 attempted to self-heal by recreating the broken sacrificed bond. Consequently, the initial strain for KaMA, K-G1 to K-G20 in 2nd cycle was 54.09, 51.16, 46.78, 39.31 and 30.40%, respectively. It could be found that none of nanocomposite hydrogels found its initial shape. Between various samples, pure KaMA hydrogel revealed the weak shape recovery. Moreover, incorporation of GOPD improved shape recovery ability of KaMA structure. By increasing amounts of GOPD content, more water was absorbed in the hydrogels leading to acceleration of self-healing rate, recreating secondary bond and also regaining the initial structure. Energy loss, the area between loading and unloading, was also evaluated for 1st and 2nd cycles (Fig. 7B). For the 1st cycle, energy loss of nanohybrid hydrogels significantly enhanced from 2.8 ± 0.10 kJ/m^3 (for KaMA) to 21.1 ± 0.53 kJ/m^3 at K-G10 sample. According to our previous results, addition of nanoparticles to the KaMA network resulted in enhanced toughness, leading to improvement of absorbed energy volume. By comparing the energy loss of KaMA (2.8 ± 0.10 kJ/m) with toughness (4.0 ± 0.15 kJ/m^3), it could be concluded that 70% of absorbed energy lost in this cycle. Same calculation for K-G20 revealed that, 61% of energy lost. Therefore, our results revealed that incorporation of GOPD not only increased ability of hydrogel's network to absorb more energy upon deformation, but also promoted the elastic-like behavior of structure to return the energy. Moreover, at K-G1, K-G4 and K-G10 samples, the energy loss of 2nd cycle was significantly less than that of 1st cycle. It could be due to low energy absorption at the second cycle leading to less energy loss. However, K-G20 hydrogel revealed different behavior. At this sample, better shape recovery of the deformed hydrogel structure resulted in the decrease in the initial strain point of the second cycle to less than 30%. Subsequently, compared to 1st cycle, the energy absorption and loss significantly increased. Moreover, based on both cycle curves of each specimen, some of specimen could recover their own strength, even if they could not recover their initial shape. Strength recovery was evaluated by comparison of area under 1st and 2nd cycles (Fig. 7C). Resulted showed that the strength recovery was significantly enhanced with increasing amount of GOPD nanoparticles, from 19% (at KaMA) to 93% (at K-G20). It might be due to the role of catechol groups to absorb more water and assist the polymeric structure to recover its own mechanical properties.

Moreover, our results revealed that the compressive strength of hydrogels (KaMA, K-G1, K-G4, K-G10 and K-G20) in the 2nd cycle was 20.9, 120.78, 150.2, 190.7 and 232.6 kPa, respectively. It could be concluded that increasing GOPD content resulted in enhanced strength in 2nd cycle compared to that of 1st one which we named them as the work-hardening phenomenon. Noticeably, while the strength of K-G20 sample at 1st cycle was estimated 171.3 ± 8.3 kPa (at 60% strain), it was enhanced to 232.6 ± 5.9 kPa at 2nd cycle. Based on these results, work-hardening energy were determined by measuring area between 1st and 2nd loading curve (Fig. 7D). Our results revealed that work-hardening energy enhanced with increasing the amounts of GOPD content from 0.13 ± 0.03 kJ/m^3 (for K-G1) to 13.9 ± 0.67 kJ/m^3 (for K-G20). It could be due to the interaction between catechol groups of GOPD and K^+ ions, in order to assist the structure to self-heal, efficiently. Catechol interaction with other moieties not only supported broken bonds in hydrogel structure to recreated in PBS solution, but also the strong interaction of catechol group with K^+ led to the formation of a strengthen interpreting network. In other research, Mihaila et al. (2013) found that increasing methacrylation degree of methacrylate κ-CA resulted in increasing energy loss. Furthermore, they found that by increasing degree of methacrylation, recovery of hydrogels was enhanced. However, they did not find any sign of work-hardening. Therefore, we concluded that this phenomenon was truly based on the interaction between GOPD and K^+ or other moieties. In another research, Thakur et al. (2016) found out the addition of nanosilica to the methacrylate κ-CA resulted in mechanically stiff and flexible network, which reduced energy loss which was different with the behavior of GOPD. The schematic presenting in Fig. 7D reveals two K-G4 hydrogels with two different red and blue colors. After 1 h setting of these hydrogels together in PBS solution, some bonds were created in the interface between two hydrogels showing its integration. After cutting the interface, we found that the interface's color changed to purple confirming the integration of these hydrogels. This fact showed that in PBS solution, nanohybrid hydrogels could recreate the broken bonds and intra-structures could heal its own network, which confirmed previous results.

In order to evaluate the behavior of K-G10 and K-G20 in 2nd cycle, the cross-section images of hydrogels after 1st cycle loading and 2-h immersing in PBS solution was investigated (Fig. 8). Lower magnification images (30×) revealed that 3D porous structure of K-G10 transformed to the deformed and aligned structure due to the catastrophic strain. It needs to mention that especially KaMA hydrogel slightly lost their integrity and consequently destroyed. Initial resistance for postponing the destruction under severe strain, and subsequently recovery of K-G10 in PBS was due to catechol groups of polydopamine. According to higher magnification images (2000×), GOPD nanoparticles with convex morphology completely covered the pore walls of KaMA as a reinforcement (red arrows), which supported KaMA to tolerate higher stress. Furthermore, the catechol groups of GOPD could interact with other moieties leading to the formation of bridges between the pore walls and improved strength of structure.

Moreover, SEM images revealed that compared to K-G10, K-G20 revealed less deformation and could better recover its structure. Moreover, red arrows revealed GOPD nanoparticles with filamentous shapes strongly interacted with wall surfaces. Furthermore, the bridges that connected the walls were increased and also were bigger with more interactions with polymeric structure, helping to create more connected network, leading to improved stability.

3.6. Cell culture

In order to evaluate the role of GOPD incorporation on the biological properties of KaMA, fibroblasts were seeded on the samples and cell proliferation and spreading on various samples were investigated. At first, cell viability on various nanohybrid hydrogels was determined by using Live/dead assay. Fig. 9A shows that after 5 days of culture, by increasing the amounts of GOPD content, the number of live cells enhanced intensely. At the specific time points, the viability of cells was evaluated by comparing the number of live cells to all cells. Cell viability on various samples is presented in Fig. 9B. The significant ascending viability during 5 days of culture showed that KaMA-GOPD nanohybrid hydrogels were biocompatible with fibroblast cells. In addition, our results revealed that, after 5 days of culture, the viability of fibroblasts enhanced from 76.3 ± 2.1%–86.7 ± 3.7%, when the hydrogel substrate was changed from KaMA to K-G1. In addition, we found that increasing amounts of GOPD content upon 20 wt.% (K-G20 sample) significantly improved cell viability (95.2 ± 1.6%) compared to K-G1 sample. It might be related to the positive role of both GO and PD in GOPD nanoparticles. According to previous results, GO nanosheets could modulate the surface chemistry and stiffness of

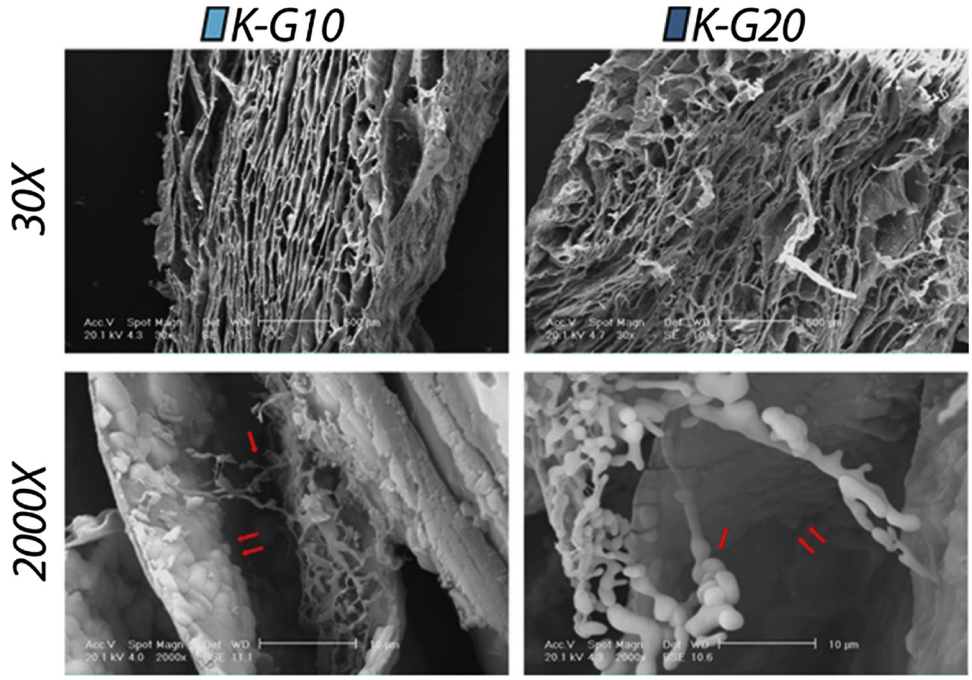

Fig. 8. SEM images of the K-G10 and K-G20 hydrogels after 1st cycle compression until 60% strain and immersing in PBS solution for 2 h at two different magnifications.

substrates leading to promotion of cell function (Halim, Luo, Ju, & Song, 2018; Wan, Frydrych, & Chen, 2011). Chen, Müller, Gilmore, Wallace, and Li (2008) also found out that graphene and its derivatives such as GO could promote the adhesion and proliferation of fibroblast cells. In a similar research, Kang et al. (2015) observed considerably improvement in the cell function with incorporation of GO to the polymeric structure due to promoted stiffness of soft environment. In addition, Zhang et al. (2011) observed, incorporation of optimized GO into polymeric hydrogels improved its mechanical properties and promoted cell viability. In another word, Tsai et al. (Tsai, Chen, Chien, Kuo, & Wang, 2011) showed that surface modification of nanoparticles with PD could result in faster proliferation of cells due to promoted immobilization of serum adhesive proteins such as fibronectin on the surface. Cell proliferation was also investigated using MTT assay during 5 days of culture (Fig. 9C). Results showed significant improvement of cell survival, during 5 days of culture. Moreover, addition of nanoparticle to KaMA hydrogel resulted in significantly enhanced cell survival (1.5-folds), from 95.4 ± 5.4% control (for KaMA) to 156.0 ± 9.9% control (for K-G1). In addition, with increasing amounts of GOPD in K-G series, survival of cells noticeably improved. Remarkably, after 5 days of culture, cell survival on the K-G20 hydrogel was estimated 241.8 ± 5.5%control, confirming live/dead assay result. Furthermore, we studied cytoskeletal organization (F-actin) of fibroblast cells on the nanohybrid hydrogels, after 5 days of culture (Fig. 9D). Actin filament staining showed that the cytoskeletal organization of the cells were considerably affected by the hydrogel's structure. While low density of cells was spread on the KaMA hydrogel, by increasing amounts GOPD content, the cells started to expand their cytoskeletal and spread over a larger area. After spreading, cells tried to form their pseudopodia on K-G series (especially K-G10 and KG-20), leading to development of bridges connections between fibroblast cells on the nanohybrid hydrogels. Previous researches showed that this behavior was related to PD, which facilitated protein adsorption and cell adhesion (Ku, Ryu, Hong, Lee, & Park, 2010; Shin, Lee, & Shin, 2011). Liu et al. (2015) found out similar cellular behavior on zirconia coated PD. To evaluate the role of substrate on the cell spreading, cell area on various hydrogels was measured (Fig. 9E). Our results revealed that the fraction of surface hydrogel covered with fibroblasts significantly improved (5.7 folds) from 15.7 ± 3.7% (at KaMA) to 90.2 ± 3.5% (at K-G20), showing the effective role of GOPD on cell spreading. KaMA hydrogels showed the lowest cell attachment and spreading, due to lack of cell binding domains on KaMA surface.

According to previous results, Cell's fate could be controlled by many chemical and physical factors of environment, named cell niche (Halim et al., 2018; Tong, Jiang, Zhu, & Yang, 2016). Between them, mechanical signals and especially stiffness played crucial role to control cell function (Jiang et al., 2016). Our results revealed that incorporation of GOPD to structure of KaMA hydrogels resulted in improved mechanical properties leading to enhanced cell adhesion and spreading. Moreover, presence of catechol groups of PD on the GO surface could effectively increase the adhesion sites to attract proteins inside culture media through electrostatically interaction leading to improved cell attachment and spreading.

4. Conclusion

In this research, we engineered an injectable shear-thinning and mechanically robust hydrogel based on Kappa-carrageenan (KaMA)-dopamine functionalized graphene oxide (GOPD) for soft tissue engineering. This hydrogel was developed using dual-crosslinking mechanism, which transmuted this hydrogel to unique biomaterials with superior properties. The presence of GOPD nanoparticle in the KaMA hydrogels allowed it to inject efficiently by enhancing shear-thinning behavior of KaMA. Furthermore, compressive strength and toughness of hydrogel were improved dramatically, giving the hydrogel potential to resist high shear stress, while showing self-healing behavior by re-creating secondary bond. Moreover, the addition of GOPD nanoparticle to KaMA matrix caused recovery properties originating from corporation of catechol group of polydopamine with other moieties. Additionally, biocompatibility of this nanohybrid hydrogel was noticeably promoted with increasing GOPD content. Accordingly, KaMA-GOPD hybrid hydrogel could be a desirable choice for soft tissue engineering and 3D bioprinting applications.

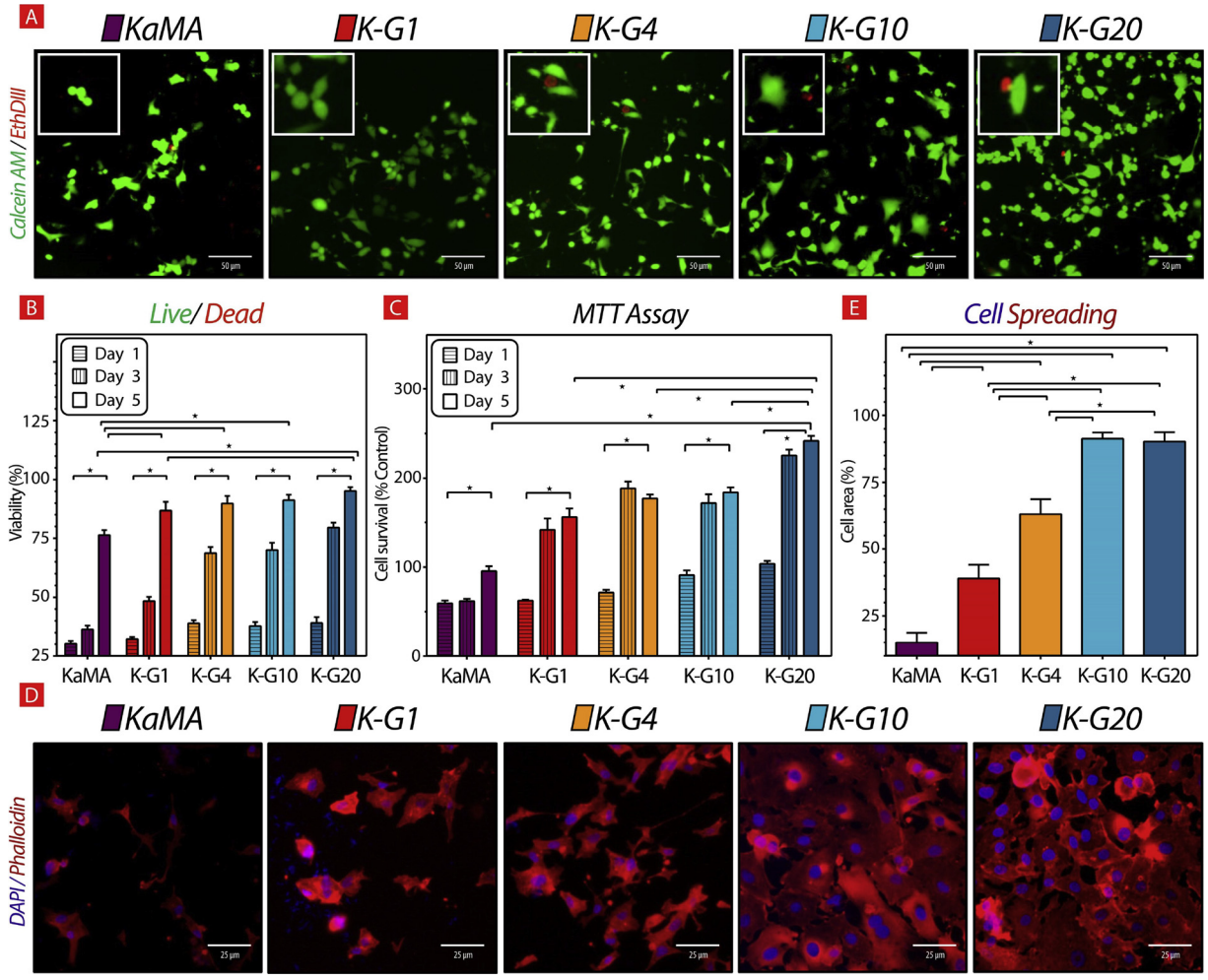

Fig. 9. A) Representative fluorescence images of live/dead assay of fibroblasts seeded on the KaMA-GOPD hydrogels at day 5 of culture (The cells stained with Calcein AM (green) and EthDII (red) presented live and dead, respectively). B) Quantified cell viability results, obtained from live/dead assay, measured at days 1, 3 and 5 of culture. C) Normalized survival of fibroblast cells cultured on various nanohybrid hydrogels measured using MTT assays during 5 days of culture. The absorbance was normalized against the control (TCP) at each time interval. D) Representative fluorescence images of the actin cytoskeleton of the fibroblasts after 5 days of culture on various samples. The nuclei and actin cytoskeleton of fibroblast were stained with DAPI (blue) and rhodamine-phalloidin (red), respectively. E) Cell spreading, the fraction of area covered with cell clusters, after 5 days of culture, on various nanohybrid hydrogels, measured via DAPI/Phalloidin assay (*: $P < 0.05$). (For interpretation of the references to colour in this figure legend, the reader is referred to the web version of this article.)

Acknowledgments

The authors should have thanked from Iran National Foundation (INSF, Grant no.93841433) and Isfahan University of Technology for the financial support. We are immensely grateful to all rheology lab's experts from Iran Polymer and Petrochemical Institute, Dr. Mohammad Hossein Ghanian from Royan Institute and Raouf Rahimzadeh from Isfahan University of Technology for their scientific and experimental support.

Appendix A. Supplementary data

Supplementary material related to this article can be found, in the online version, at doi:https://doi.org/10.1016/j.carbpol.2019.03.030.

References

Abad, L. V., Saiki, S., Nagasawa, N., Kudo, H., Katsumura, Y., & De La Rosa, A. M. (2011). NMR analysis of fractionated irradiated κ-carrageenan oligomers as plant growth promoter. *Radiation Physics and Chemistry, 80*(9), 977–982.

Campo, V. L., Kawano, D. F., Silva, D. B. D., & Carvalho, I. (2009). Carrageenans: Biological properties, chemical modifications and structural analysis—A review. *Carbohydrate Polymers, 77*(2), 167–180.

Centeno, S. A., & Shamir, J. (2008). Surface enhanced Raman scattering (SERS) and FTIR characterization of the sepia melanin pigment used in works of art. *Journal of Molecular Structure, 873*(1–3), 149–159.

Chen, H., Müller, M. B., Gilmore, K. J., Wallace, G. G., & Li, D. (2008). Mechanically strong, electrically conductive, and biocompatible graphene paper. *Advanced Materials, 20*(18), 3557–3561.

Cheng, C., Li, S., Nie, S., Zhao, W., Yang, H., Sun, S., & Zhao, C. (2012). General and biomimetic approach to biopolymer-functionalized graphene oxide nanosheet through adhesive dopamine. *Biomacromolecules, 13*(12), 4236–4246.

Cheng, C., Nie, S., Li, S., Peng, H., Yang, H., Ma, L., ... Zhao, C. (2013). Biopolymer functionalized reduced graphene oxide with enhanced biocompatibility via mussel inspired coatings/anchors. *Journal of Materials Chemistry B, 1*(3), 265–275.

Chung, H., Kim, Y., Shin, D., Ryoo, S., Hong, B. H., & Min, D. (2013). Biomedical applications of graphene and graphene oxide. *Accounts of Chemical Research, 46*(10), 2211–2224.

Colinet, I., Dulong, V., Mocanu, G., Picton, L., & Le Cerf, D. (2010). Effect of chitosan coating on the swelling and controlled release of a poorly water-soluble drug from an amphiphilic and pH-sensitive hydrogel. *International Journal of Biological Macromolecules, 47*(2), 120–125.

Coutinho, D. F., Sant, S. V., Shin, H., Oliveira, J. T., Gomes, M. E., Neves, N. M., ... Reis, R. L. (2010). Modified Gellan Gum hydrogels with tunable physical and mechanical properties. *Biomaterials, 31*(29), 7494–7502.

Cross, L. M., Shah, K., Palani, S., Peak, C. W., & Gaharwar, A. K. (2018). Gradient nanocomposite hydrogels for interface tissue engineering. *Nanomedicine, 14*(7), 2465–2474.

Daniel-da-Silva, A. L., Moreira, J., Neto, R., Estrada, A. C., Gil, A. M., & Trindade, T. (2012). Impact of magnetic nanofillers in the swelling and release properties of κ-carrageenan hydrogel nanocomposites. *Carbohydrate Polymers, 87*(1), 328–335.

Das, S., Irin, F., Ma, L., Bhattacharia, S. K., Hedden, R. C., & Green, M. J. (2013). Rheology

and morphology of pristine graphene/polyacrylamide gel. *ACS Applied Materials & Interfaces, 5*(17), 8633–8640.
Del Giudice, F., & Shen, A. Q. (2017). Shear rheology of graphene oxide dispersions. *Chemical Engineering, 16*, 23–30.
Diba, M., Pape, B., Klymov, A., Zhang, Y., Song, J., Lowik, D., ... Leeuwenburgh, S. C. G. (2017). Nanostructured raspberry-like gelatin microspheres for local delivery of multiple biomolecules. *Acta Biomaterialia, 58*, 67–79.
Diba, M., Wang, H., Kodger, T. E., Parsa, S., & Leeuwenburgh, S. C. (2017). Highly elastic and self-healing composite colloidal gels. *Advanced Materials, 29*(11).
Eigler, S., Dotzer, C., & Hirsch, A. (2012). Visualization of defect densities in reduced graphene oxide. *Carbon, 50*(10), 3666–3673.
Fang, S., Huang, D., Lv, R., Bai, Y., Huang, Z.-H., Gu, J., & Kang, F. (2017). Three-dimensional reduced graphene oxide powder for efficient microwave absorption in the S-band (2–4 GHz). *RSC Advances, 7*(41), 25773–25779.
Ferrari, A. C., Meyer, J. C., Scardaci, V., Casiraghi, C., Lazzeri, M., Mauri, F., ... Geim, A. K. (2006). Raman spectrum of graphene and graphene layers. *Physical Review Letters, 97*(18), 187401.
Fu, L., Lai, G., Jia, B., & Yu, A. (2014). Preparation and electrocatalytic properties of polydopamine functionalized reduced graphene oxide-silver nanocomposites. *Electrocatalysis, 6*(1), 72–76.
Gaharwar, A. K., Schexnailder, P., Kaul, V., Akkus, O., Zakharov, D., Seifert, S., & Schmidt, G. (2010). Highly extensible bio-nanocomposite films with direction-dependent properties. *Advance Functional Material, 20*, 429–436.
Guvendiren, M., Lu, H. D., & Burdick, J. A. (2012). Shear-thinning hydrogels for biomedical applications. *Soft Matter, 8*(2), 260–272.
Halim, A., Luo, Q., Ju, Y., & Song, G. (2018). A mini review focused on the recent applications of graphene oxide in stem cell growth and differentiation. *Nanomaterials (Basel), 8*(9).
Han, L., Lu, X., Liu, K., Wang, K., Fang, L., Weng, L. T., ... Li, Z. (2017). Mussel-inspired adhesive and tough hydrogel based on nanoclay confined dopamine polymerization. *ACS Nano, 11*(3), 2561–2574.
Huanga, Y., Zenga, M., Rena, J., Wanga, J., Fana, L., & Xu, Q. (2012). Preparation and swelling properties of graphene oxidepoly(acrylic acid-co-acrylamide) super-absorbent hydrogel nanocomposites. *Colloids and Surfaces A: Physicochemical and Engineering Aspects, 401*, 97–106.
Hwang, S., Kang, D., Ruoff, R. S., Shin, H. S., & Park, Y. (2014). Poly(vinyl alcohol) reinforced and toughened with poly(dopamine)-treated graphene oxide, and its use for humidity sensing. *American Chemical Society, 8*(7), 6739–6747.
Jiang, L., Sun, Z., Chen, X., Li, J., Xu, Y., Zu, Y., ... Yang, C. (2016). Cells sensing mechanical cues: Stiffness influences the lifetime of cell-extracellular matrix interactions by affecting the loading rate. *ACS Nano, 10*(1), 207–217.
Jiao, G., Yu, G., Zhang, J., & Ewart, H. (2011). Chemical structures and bioactivities of sulfated polysaccharides from marine algae. *Marine Drugs, 9*(2), 196–223.
Jing, Y., Yuan, X., Yuan, Q., He, K., Liu, Y., Lu, P., ... Li, G. (2016). Determination of nicotine in tobacco products based on mussel-inspired reduced graphene oxide-supported gold nanoparticles. *Scientific Reports, 6*, 29230.
Jing, X., Mi, H.-Y., Napiwocki, B. N., Peng, X.-F., & Turng, L.-S. (2017). Mussel-inspired electroactive chitosan/graphene oxide composite hydrogel with rapid self-healing and recovery behavior for tissue engineering. *Carbon, 125*, 557–570.
Kang, S., Park, J. B., Lee, T.-J., Ryu, S., Bhang, S. H., La, W.-G., ... Kim, B.-S. (2015). Covalent conjugation of mechanically stiff graphene oxide flakes to three-dimensional collagen scaffolds for osteogenic differentiation of human mesenchymal stem cells. *Carbon, 83*, 162–172.
Keller, D. S., Tahilramani, R. N., Flores-Gonzalez, J. R., Mahmood, A., & Haas, E. M. (2016). Transanal minimally invasive surgery: Review of indications and outcomes from 75 consecutive patients. *Journal of the American College of Surgeons, 222*(5), 814–822.
Kim, J. E., & Lee, H. S. (2014). Oscillatory shear induced gelation of graphene-poly(vinyl alcohol) composite hydrogels and rheological premonitor of ultra-light aerogels. *Polymer, 55*, 287–294.
Kretlow, J. D., Klouda, L., & Mikos, A. G. (2007). Injectable matrices and scaffolds for drug delivery in tissue engineering. *Advanced Drug Delivery Reviews, 59*(4–5), 263–273.
Ku, S. H., Ryu, J., Hong, S. K., Lee, H., & Park, C. B. (2010). General functionalization route for cell adhesion on non-wetting surfaces. *Biomaterials, 31*(9), 2535–2541.
Kuo, C. K., & Ma, P. X. (2008). Maintaining dimensions and mechanical properties of ionically crosslinked alginate hydrogel scaffolds in vitro. *Journal of Biomedical Materials Research Part A, 84*(4), 899–907.
Lee, H., Dellatore, S. M., Miller, W. M., & Messersmith, P. B. (2007). Mussel-inspired surface chemistry for multifunctional coatings. *Science, 318*, 426–430.
Liang, Y. J., Zhen, J., Chen, N., & Reith, M. E. (2009). Interaction of catechol and non-catechol substrates with externally or internally facing dopamine transporters. *Journal of Neurochemistry, 109*(4), 981–994.
Liao, J., Qu, Y., Chu, B., Zhang, X., & Qian, Z. (2015). Biodegradable CSMA/PECA/graphene porous hybrid scaffold for cartilage tissue engineering. *Scientific Reports, 5*, 9879.
Liu, H., Xi, P., Xie, G., Shi, Y., Hou, F., Huang, L., ... Wang, J. (2012). Simultaneous reduction and surface functionalization of graphene oxide for hydroxyapatite mineralization. *The Journal of Physical Chemistry C, 116*(5), 3334–3341.
Liu, M., Zhou, J., Yang, Y., Zheng, M., Yang, J., & Tan, J. (2015). Surface modification of zirconia with polydopamine to enhance fibroblast response and decrease bacterial activity in vitro: A potential technique for soft tissue engineering applications. *Colloids and Surfaces B: Biointerfaces, 136*, 74–83.
Loebel, C., Rodell, C. B., Chen, M. H., & Burdick, J. A. (2017). Shear-thinning and self-healing hydrogels as injectable therapeutics and for 3D-printing. *Nature Protocols, 12*(8), 1521–1541.
Lokhande, G., Carrow, J. K., Thakur, T., Xavier, J. R., Parani, M., Bayless, K. J., & Gaharwar, A. K. (2018). Nanoengineered injectable hydrogels for wound healing application. *Acta Biomaterialia, 70*, 35–47.
Luo, J., Jiang, S., & Liu, X. (2013). Efficient one-pot synthesis of mussel-inspired molecularly imprinted polymer coated graphene for protein-specific recognition and fast separation. *The Journal of Physical Chemistry C, 117*(36), 18448–18456.
Ma, Y., Niu, H., Zhang, X., & Cai, Y. (2011). One-step synthesis of silver/dopamine nanoparticles and visual detection of melamine in raw milk. *Analyst, 136*(20), 4192–4196.
Marcano, D. C., Kosynkin, D. V., Berlin, J. M., Sinitskii, A., Sun, Z., Slesarev, A., ... Tour, J. M. (2010). Improved synthesis of graphene oxide. *ACS Nano, 4*(8), 4806–4814.
Mihaila, S. M., Gaharwar, A. K., Reis, R. L., Marques, A. P., Gomes, M. E., & Khademhosseini, A. (2013). Photocrosslinkable kappa-carrageenan hydrogels for tissue engineering applications. *Advanced Healthcare Materials, 2*(6), 895–907.
Mihaila, S. M., Popa, E. G., Reis, R. L., Marques, A. P., & Gomes, M. E. (2014). Fabrication of endothelial cell-laden carrageenan microfibers for microvascularized bone tissue engineering applications. *Biomacromolecules, 15*(8), 2849–2860.
Mobarak, N. N., Ramli, N., Ahmad, A., & Rahman, M. Y. A. (2012). Chemical interaction and conductivity of carboxymethyl κ-carrageenan based green polymer electrolyte. *Solid State Ionics, 224*, 51–57.
Mokhtari, H., Ghasemi, Z., Kharaziha, M., Karimzadeh, F., & Alihosseini, F. (2018). Chitosan-58S bioactive glass nanocomposite coatings on TiO2 nanotube: Structural and biological properties. *Applied Surface Science, 441*, 138–149.
Mu, J., Hou, C., Wang, H., Li, Y., Zhang, Q., & Zhu, M. (2015). Origami-inspired active graphene-based paper for programmable instant self-folding walking devices. *Science Advances, 1*(10).
Navarro, D. A., & Stortz, C. A. (2003). Determination of the configuration of 3,6-anhydrogalactose and cyclizable α-galactose 6-sulfate units in red seaweed galactans. *Carbohydrate Research, 338*(20), 2111–2118.
Necas, J., & Bartosikova, L. (2013). Carrageenan a review. *Veterinarni Medicina, 58*(4), 187–205.
Paul, A., Hasan, A., Kindi, H. A., Gaharwar, A. K., Rao, V. T., Nikkhah, M., ... Khademhosseini, A. (2014). Injectable graphene oxide hydrogel-based angiogenic gene delivery system for vasculogenesis and cardiac repair. *American Chemical Society, 8*(8), 8050–8062.
Phua, S. L., Yang, L., Toh, C. L., Huang, S., Tsakadze, Z., Lau, S. K., ... Lu, X. (2012). Reinforcement of polyether polyurethane with dopamine-modified clay: The role of interfacial hydrogen bonding. *ACS Applied Materials & Interfaces, 4*(9), 4571–4578.
Pittet, B., Montandon, D., & Pittet, D. (2005). Infection in breast implants. *The Lancet Infectious Diseases, 5*(2), 94–106.
Popa, E. G., Caridade, S. G., Mano, J. F., Reis, R. L., & Gomes, M. E. (2015). Chondrogenic potential of injectable kappa-carrageenan hydrogel with encapsulated adipose stem cells for cartilage tissue-engineering applications. *Journal of Tissue Engineering and Regenerative Medicine, 9*(5), 550–563.
Popuri, S. R., Harris-Logie, A., Lino, K. H., Cadogan, E. I., & Lee, C.-H. (2014). Evaluation of antibacterial activity and characterization of synthesized biodegradable copolymers. *Polymer-Plastics Technology and Engineering, 53*(15), 1625–1635.
Rnjak-Kovacina, J., Wray, L. S., Burke, K. A., Torregrosa, T., Golinski, J. M., Huang, W., & Kaplan, D. L. (2015). Lyophilized silk sponges: A versatile biomaterial platform for soft tissue engineering. *ACS Biomaterials Science & Engineering, 1*(4), 260–270.
Schönfelder, R., Rümmeli, M. H., Gruner, W., Löffler, M., Acker, J., Hoffmann, V., ... Pichler, T. (2007). Purification-induced sidewall functionalization of magnetically pure single-walled carbon nanotubes. *Nanotechnology, 18*(37), 375601.
Shin, S. R., Aghaei-Ghareh-Bolagh, B., Gao, X., Nikkhah, M., Jung, S. M., Dolatshahi-Pirouz, A., ... Khademhosseini, A. (2014). Layer-by-layer assembly of 3D tissue constructs with functionalized graphene. *Advanced Functional Materials, 24*(39), 6136–6144.
Shin, Y. M., Lee, Y. B., & Shin, H. (2011). Time-dependent mussel-inspired functionalization of poly(L-lactide-co-varepsilon-caprolactone) substrates for tunable cell behaviors. *Colloids and Surfaces B: Biointerfaces, 87*(1), 79–87.
Stratton, S., Manoukian, O. S., Patel, R., Wentworth, A., Rudraiah, S., & Kumbar, S. G. (2018). Polymeric 3D printed structures for soft-tissue engineering. *Journal of Applied Polymer Science, 135*(24).
Su, Z., Wang, H., Tian, K., Huang, W., Guo, Y., He, J., & Tian, X. (2018). Multifunctional anisotropic flexible cycloaliphatic epoxy resin nanocomposites reinforced by aligned graphite flake with non-covalent biomimetic. *Composites Part A: Applied Science and Manufacturing, 109*, 472–480.
Tan, F., Liu, M., & Ren, S. (2017). Preparation of polydopamine-coated graphene oxide/Fe3O4 imprinted nanoparticles for selective removal of fluoroquinolone antibiotics in water. *Scientific Reports, 7*(1), 5735.
Thakur, A., Jaiswal, M. K., Peak, C. W., Carrow, J. K., Gentry, J., Dolatshahi-Pirouz, A., & Gaharwar, A. K. (2016). Injectable shear-thinning nanoengineered hydrogels for stem cell delivery. *Nanoscale, 8*(24), 12362–12372.
Thanusha, A. V., Dinda, A. K., & Koul, V. (2018). Evaluation of nano hydrogel composite based on gelatin/HA/CS suffused with asiatic acid/ZnO and CuO nanoparticles for second degree burns. *Materials Science & Engineering C: Materials for Biological Applications, 89*, 378–386.
Tong, X., Jiang, J., Zhu, D., & Yang, F. (2016). Hydrogels with dual gradients of mechanical and biochemical cues for deciphering cell-niche interactions. *ACS Biomaterials Science & Engineering, 2*(5), 845–852.
Tsai, W. B., Chen, W. T., Chien, H. W., Kuo, W. H., & Wang, M. J. (2011). Poly(dopamine) coating of scaffolds for articular cartilage tissue engineering. *Acta Biomaterialia, 7*(12), 4187–4194.
Vunjak-Novakovic, G., Tandon, N., Godier, A., Maidhof, R., Marsano, A., Martens, T. P., & Radisic, M. (2010). Challenges in cardiac tissue engineering. *Tissue Engineering: Part B, 16*(2).

Wan, C., Frydrych, M., & Chen, B. (2011). Strong and bioactive gelatin–graphene oxide nanocomposites. *Soft Matter, 7*(13), 6159.
Wang, Q., Wang, J., Lu, Q., Detamore, M. S., & Berkland, C. (2010). Injectable PLGA based colloidal gels for zero-order dexamethasone release in cranial defects. *Biomaterials, 31*(18), 4980–4986.
Xing, R., Wang, W., Jiao, T., Ma, K., Zhang, Q., Hong, W., ... Peng, Q. (2017). Bioinspired polydopamine sheathed nanofibers containing carboxylate graphene oxide nanosheet for high-efficient dyes scavenger. *ACS Sustainable Chemistry & Engineering, 5*(6), 4948–4956.
Xiong, S., Wang, Y., Yu, J., Chen, L., Zhu, J., & Hu, Z. (2014). Polydopamine particles for next-generation multifunctional biocomposites. *Journal of Materials Chemistry A, 2*(20), 7578–7587.
Xu, L. Q., Yang, W. J., Neoh, K., Kang, E., & Fu, G. D. (2010). Dopamine-induced reduction and functionalization of graphene oxide nanosheets. *Macromolecules, 43*, 8336–8339.
Xu, F., Xie, S., Cao, R., Feng, Y. N., Ren, C., & Wang, L. (2017). Prepare poly-dopamine coated graphene@silver nanohybrid for improved surface enhanced Raman scattering detection of dyes. *Sensors and Actuators B: Chemical, 243*, 609–616.
Yamaguchi, H., Eda, G., Mattevi, C., Kim, H., & Chhowalla, M. (2010). Highly uniform 300 mm wafer-scale deposition of single and multilayered chemically derived graphene thin films. *ACS Nano, 4*(1), 524–528.
Yang, B., Zhang, Y., Zhang, X., Tao, L., Lia, S., & Wei, W. (2012). Facilely prepared inexpensive and biocompatible self-healing hydrogel: A new. *Polymer Chemistry, 3*(12), 3235–3238.
Yang, J., Zhang, Y. S., Yue, K., & Khademhosseini, A. (2017). Cell-laden hydrogels for osteochondral and cartilage tissue engineering. *Acta Biomaterialia, 57*, 1–25.
Ye, W., Shi, X., Su, J., Chen, Y., Fu, J., Zhao, X., ... Xue, D. (2014). One-step reduction and functionalization protocol to synthesize polydopamine wrapping Ag/graphene hybrid for efficient oxidation of hydroquinone to benzoquinone. *Applied Catalysis B: Environmental, 160–161*, 400–407.
Yegappan, R., Selvaprithiviraj, V., Amirthalingam, S., Mohandas, A., Hwang, N. S., & Jayakumar, R. (2019). Injectable angiogenic and osteogenic carrageenan nanocomposite hydrogel for bone tissue engineering. *International Journal of Biological Macromolecules, 122*, 320–328.
Yu, L., & Ding, J. (2008). Injectable hydrogels as unique biomedical materials. *Chemical Society Reviews, 37*(8), 1473–1481.
Yu, M., Song, A., Xu, G., Xin, X., Shen, J., Zhang, H., & Song, Z. (2015). 3D welan gum–graphene oxide composite hydrogels with efficient dye adsorption capacity. *RSC Advances, 5*(92), 75589–75599.
Yuksel, E., Choo, J., Wettergreen, M., & Liebschner, M. (2005). *Challenges in soft tissue engineering, seminars in plastic surgery, Vol. 19*, 333 Seventh Avenue, New York, NY 10001, USA: Thieme Medical Publishers, Inc261–270.
Zangmeister, R. A., Morris, T. A., & Tarlov, M. J. (2013). Characterization of polydopamine thin films deposited at short times by autoxidation of dopamine. *Langmuir, 29*(27), 8619–8628.
Zhang, L., Wang, Z., Xu, C., Li, Y., Gao, J., Wang, W., & Liu, Y. (2011). High strength graphene oxide/polyvinyl alcohol composite hydrogels. *Journal of Materials Chemistry, 21*(28), 10399.
Zhao, W., Fang, M., Wu, F., Wu, H., Wang, L., & Chen, G. (2010). Preparation of graphene by exfoliation of graphite using wet ball milling. *Journal of Materials Chemistry, 20*(28), 5817.
Zheng, Q., Zhang, B., Lin, X., Shen, X., Yousefi, N., Huang, Z.-D., ... Kim, J.-K. (2012). Highly transparent and conducting ultralarge graphene oxide/single-walled carbon nanotube hybrid films produced by Langmuir–Blodgett assembly. *Journal of Materials Chemistry, 22*(48), 25072.
Zhu, W., Chen, T., Li, Y., Lei, J., Chen, X., Yao, W., & Duan, T. (2017). High performances of artificial nacre-like graphene oxide-carrageenan bio-nanocomposite films. *Materials (Basel), 10*(5).